Investigation of fires in a mechanically ventilated compartment using the CFD code FireFOAM

Okorie Ukairo[1], Siaka Dembele[1*], Ali Heidari[1], Hugues Pretrel[2], Jennifer Wen[3]

[1]Department of Mechanical Engineering, Kingston University London SW15 3DW, UK

[2]Institut de Radioprotection et de Sûreté Nucléaire (IRSN), Saint Paul Lez Durance, France

[3]School of Engineering, University of Warwick, Coventry CV4 9YP, UK

*corresponding author: s.dembele@kingston.ac.uk

Abstract

The outbreak of fires in nuclear power plants is a major risk due to the potential leak of radioactive materials. The use of traditional prescriptive fire safety regulations has shown its limitations and there is now a shift towards performance-based fire safety engineering, which requires well-validated fire models. Nuclear power plants require the use of mechanical ventilation, which provides dynamic confinement for nuclear materials by maintaining the required pressure. The occurrence of fires could potentially result in pressure variations within power plants. Although dynamic confinement along with other safety measures are in place to prevent fires, there is a continuous need to assess fire safety measures and reduce the risk of fire propagation with the use of fire simulation codes.

The current study aims to build on existing research by making use of an emerging open-source computational fluid dynamics (CFD) fire simulation code known as FireFOAM, to predict fire behaviour in a mechanically ventilated nuclear compartment. An existing in-house modified version of FireFOAM developed by the authors' research group, is further modified in the present work to include a Conjugate Heat Transfer (CHT) model to account for the heat transfer between combustion gases and solid boundaries. The CHT is validated using the experimental wall temperatures and heat fluxes. Furthermore, a mechanical ventilation model has been developed and implemented into FireFOAM. This newly modified version of FireFOAM is employed to predict the pressure variations in a nuclear compartment and the flow rates in the ventilation network. The predictions are compared to some experimental data from the open literature. Overall, it is shown that the mechanical ventilation model and the modified FireFOAM with CHT can predict the pressure variations and flow rates with a relatively good level of accuracy.

Keywords:

Fire; Computational Fluid Dynamics; Mechanical Ventilation Model; FireFOAM

Nomenclature

D	Species laminar diffusion coefficient $\left(\frac{m^2}{s}\right)$
g_i	Gravity in the ith direction $(\frac{m}{s^2})$
h	Enthalpy (J/kg)
p	Pressure (Pa)
Pr_t	Prandtl number
Q	Heat source (W)
$\dot{q}'''$	Heat release rate per unit volume $\left(\frac{\mathrm{J}}{\mathrm{m}^3}\right)$
$\dot{q}_r''$	Radiative heat flux $\left(\frac{\mathrm{W}}{\mathrm{m}^2}\right)$
S	Longitudinal source term
Sc_t	Turbulent Schmidt number
T	Temperature (K)
t	Time (s)
u_j	Cartesian Velocity (m/s)
x_j	Cartesian Length (m)
Y_m	Mass fraction of species m

Greek

ρ	Density $\left(\frac{kg}{m^3}\right)$
x	Longitudinal coordinate (m)
υ	Kinematic viscosity $\left(\frac{m^2}{s}\right)$
υ_t	Turbulent viscosity $\left(\frac{m^2}{s}\right)$
α	Thermal laminar diffusion coefficient $\left(\frac{m^2}{s}\right)$
$\bar{\omega}_{m,g}$	Mean reaction rate (ms^{-1})
λ_s	Thermal conductivity $\left(\frac{W}{mK}\right)$
λ_{eff}	Effective thermal conductivity $\left(\frac{W}{mK}\right)$

σ Stefan-Boltzmann constant ($5.67\ x10^{-8}\ Wm^{-2}K^{-4}$)

∇ nabla-operator $\left(\frac{\partial}{\partial x}, \frac{\partial}{\partial y}, \frac{\partial}{\partial z}\right)$

Subscripts

f Liquid

s Solid

y Local coordinate normal to the solid

1. Introduction

Nuclear facilities are equipped with mechanical ventilation networks that create dynamic confinement and control any possible release of radioactive materials during a fire outbreak (Jiang et al., 2002). In 2016, the Nuclear Energy Agency recorded 448 fire events from its twelve member countries at a varying period of observations for each member country, with the oldest observation start time of 1981 (NEA, 2016). Fires in nuclear facilities, therefore, are a significant threat to nuclear safety. During fires, pressure variations would occur due to the high level of confinement. This may lead to the loss of dynamic confinement due to the internal pressure exceeding the external pressure, resulting in emissions of radioactive materials. Because of the complex nature of fires in nuclear facilities, Computational Fluid Dynamics (CFD) tools are becoming useful approaches to describe fire behaviour**.** However, to validate this CFD approach, experimental studies are necessary to verify the accuracy of the numerical models and help further improve the existing numerical models.

In order to study the behaviour of fires in a nuclear compartment, the OECD PRISME (PRopagation d'un Incendie pour des Scenarios Multi-locaux Elementaires) fire research programme investigated the interaction between fire and mechanical ventilation in confined compartments. The experimental project PRISME 1 (Audouin et al., 2013) was conducted at the French "Institut de Radioprotection et de Sûreté Nucléaire" (IRSN) between 2007 and 2011, and consisted of full-scale experimental fire studies in a nuclear compartment. Four different test campaigns, named Source, Door, Leak, and Integral were performed during this research. PRISME "Source" investigated the fire behaviour in a single confined mechanically ventilated compartment with one burning pool fire. PRISME "Door" was concerned with the propagation of smoke and combustion products through confined and mechanically ventilated compartments with two- and three-rooms scenarios, where

one room contained the pool fire. PRISME “Leak” investigated the leakage between a fire room and adjacent compartment through slots, openings and closed doors. Finally, PRISME “Integral” examined single confined ventilated compartments with a single pool fire, looking at the propagation of gases and combustion through doorways, the behaviour of cable fires, and the effects of sprinklers and fire dampers.

Various numerical studies have been conducted using the data generated from the PRISME experiments focusing mainly on the modelling of the ventilation system and the burning rate in a vitiated environment. Considering only CFD approaches, mainly three simulation codes have been compared to the PRISME database: Fire Dynamic simulator (FDS), the in-house ISIS code of IRSN, and FireFOAM. Regarding FDS, Wahlqvist and Van Hees (2013) made use of a heating ventilation and air conditioning (HVAC) model to simulate PRISME Source, PRISME Door, and PRISME Leak experiments. Pressure inside the compartment and volume flow rate in the ventilation system were predicted with reasonable accuracy. The authors also proposed to predict the burning rate of pool fires and the effect of oxygen vitiation with an acceptable agreement (Wahlqvist and Van Hees, 2016). Sikanen and Hostikka (2017) proposed a full prediction of the burning rate including the modelling of the liquid fuel. FDS has also been used to model the ventilation system of non-PRISME tests containing mechanical ventilation. Acherar et al. (2020) studied the impact of air intake position on mechanically ventilated compartments and reported that at a low air intake position, fire grows much faster, while at a high intake positon the heat release rate reduces by a factor of 40%. With regards to the IRSN ISIS code, Bonte et al. (2013) simulated a single fire room test (PRISME Source) with an inlet and exhaust ventilation duct. Reasonable agreements were obtained for the volume flow rate in the ventilation system and pressure inside the compartment. Other authors proposed simulations of PRISME fire tests with ISIS code, predicting the airflow in the ventilation network as well as the pressure variation in the compartment. Results demonstrated the capability of the generalized Bernouilli formulation to capture the variations of flow rates and pressure during fire tests (Nasr et al., 2011; Suard et al., 2011, 2013; Lapuerta et al., 2012; Perez Segovia et al., 2017). Regarding FireFOAM code, only Le et al. (2017) investigated the ability of the original publicly available version of FireFOAM to predict fire growth by focusing on temperature, species, pressure and velocity. The combustion model in this original version of FireFOAM is based on the standard Eddy Dissipation Concept (EDC) and a grey mean absorption-emission model for species

absorption coefficient was employed (Le et al., 2017). The authors made use of PRISME Integral Test experiment with three-room fire scenarios and predicted the physical quantities with a good level of accuracy. However, in their study (Le et al., 2017), values of the flow rate in the ventilation duct were not predicted but taken from the experimental values as boundary conditions. In contrast, in the current study, the flow rate in the ventilation duct is predicted using a model. To the authors' knowledge, it is the first time a mechanical ventilation model is coupled with FireFOAM to simulate the PRISME fire experiments.

In the present study, the authors employ an existing in-house FireFOAM version, based on an extended EDC concept for combustion and a banded approach of the weighted-sum-of-gray-gas (WSGG) for radiative properties, developed through previous researches in the group. This in-house FireFOAM has been further modified as part of the present study to include Conjugate Heat Transfer (CHT) and a ventilation model. The use of CHT represents a different method from previous studies when analysing multidimensional heat transfer in the walls. Previous studies have mainly focused on the gas phase and looked at the temperature difference between the wall and the gas phase by making use of the 1D Fourier conduction equation. CHT allows for the coupling and interaction of the wall as a solid region with the gas phase. A ventilation model has also been developed as part of the current research and implemented into the in-house version of FireFOAM. The difference between the formulation of the ventilation model implemented in this study and the ventilation model implemented in FDS lies in the governing equations, construction of the computational grid and discretization techniques. These differences are briefly mentioned in the next section of this paper. The current ventilation model and the one in FDS calculate the resistance of the ventilation duct differently from ISIS.

The main goal of the present study is to assess the capability of a modified in-house version of FireFOAM that includes CHT and a ventilation model, to predict pressure variations in a typical nuclear mechanically ventilated room during fire. The current study also aims to validate a CHT approach and highlights the significance of using the CHT model which is a novel approach to the study of heat transfer in nuclear compartments. The work also has a goal to shed some light on the flow rate variations in the ventilation system.

2. Mathematical and Computational methods

FireFOAM is a fully compressible large eddy simulation (LES) code that discretizes the governing equations using the finite volume method (FVM). FireFOAM employs a Favre-

filtered fully compressible flow formulation and solves for the Navier-Stokes Equations and transport equations for species mass fractions alongside sensible enthalpy (FM Global, n.d.). The FireFOAM code was developed by FM Global for modelling large scale fires, capturing fire growth and extinction. The sensible enthalpy equation is solved in its averaged form suitable for the large eddy simulation approach. The over-bars on the equation stand for spatial filtering while the tildes stand for Favre averaging. The filtered Navier-Stokes equation for the continuity equation is given as:

$$\frac{\partial \bar{\rho}}{\partial t} + \frac{\partial \bar{\rho}\tilde{u}_j}{\partial x_j} = 0 \tag{1}$$

The filtered momentum equation is:

$$\frac{\partial \bar{\rho}\tilde{u}_i}{\partial t} + \frac{\partial \bar{\rho}\tilde{u}_i\tilde{u}_j}{\partial x_j} = -\frac{\partial \bar{p}}{\partial x_i} + \frac{\partial}{\partial x_j}\left(\bar{\rho}(v + v_t)\left(\frac{\partial \tilde{u}_i}{\partial x_j} + \frac{\partial \tilde{u}_j}{\partial x_i} - \frac{2}{3}\frac{\partial \tilde{u}_k}{\partial x_k}\delta_{ij}\right)\right) + \bar{\rho}g_i, \tag{2}$$

$$(i, j, k = 1,2,3)$$

$$\delta_{ij} = \begin{cases} 1 & i = j \\ 0 & i \neq j \end{cases}$$

The energy equation is given as:

$$\frac{\partial \bar{\rho}\tilde{h}_s}{\partial t} + \frac{\partial \bar{\rho}\tilde{h}_s\tilde{u}_j}{\partial x_j} = \frac{D\bar{p}}{Dt} + \frac{\partial}{\partial x_j}\left(\bar{\rho}\left(\alpha + \frac{v_t}{Pr_t}\right)\frac{\partial \tilde{h}_s}{\partial x_j}\right) + \dot{q}''' - \nabla \cdot \dot{q}_r'' \tag{3}$$

The gas species governing equation is expressed as:

$$\frac{\partial \bar{\rho}\tilde{Y}_m}{\partial t} + \frac{\partial \bar{\rho}\tilde{Y}_m\tilde{u}_j}{\partial x_j} = \frac{\partial}{\partial x_j}\left(\bar{\rho}\left(D + \frac{v_t}{S_{C_t}}\right)\frac{\partial \tilde{Y}_m}{\partial x_j}\right) + \bar{\omega}_{m,g} \tag{4}$$

$$(m = fuel, O_2, CO_2, H_2O)$$

where $\bar{\omega}_{m,g}$ is the mean reaction rate.

The current simulations were carried out using an in-house version of FireFOAM, in which a ventilation model was implemented in the frame of the present study. The combustion model employed in this in-house version of FireFOAM was developed by Chen at al. (2014) by extending the standard Eddy Dissipation Concept of Magnusen and Hjertager (1977) to the LES framework. The model assumes that structure levels exist under the filter width in the turbulent energy cascade from the Kolmogorov to the integral scale. The total kinetic energy and dissipation rate are derived from the subgrid-scale quantities. The combustion model assumes infinitely fast chemistry to control the filtered reaction rate by turbulent mixing rate between the fine structures located at Kolmogorov scales and the surrounding fluids. The turbulence model used is the one equation eddy viscosity model (Menom et al., 1996) for sub-grid scale closure.

The radiation heat transfer model used in our in-house version of FireFOAM is based on the modified finite-volume radiation solver fvDOM developed by Sikic (Sikic, 2018; Sikic et al., 2019) by implementing a banded approach of the weighted sum of grey gases (WSGG) model to account for gas thermal radiation absorption and emission. The modified radiation model, called "fvDOMBand" includes banded or non-grey WSGG solutions of the radiative transfer equation (RTE). The concept of the WSGG is to approximate the total emissivity of a real gas by a weighted sum of emissivities of a limited number of fictitious grey gases. There are three WSGG variants in the in-house FireFOAM which are based on the parametric database of Smith et al. (1982), Cassol et al. (2014), and Johansson et al. (2011). The parametric databases provide the WSGG pressure-absorption coefficients and the weighting coefficients, which are used in solving the RTE. In the present study, the parametric database of Smith et al. (1982) was used because it is the fastest and as accurate as other more recent databases (Cassol et al., 2014; Johansson et al., 2011). It is worth noting that our in-house version of FireFOAM is different from the standard version used by Le et al. (2017) in terms of modelling combustion, gas radiative properties and dealing with the ventilation.

It is important to point out some of the differences and similarities between the current FireFOAM code, FDS and ISIS. FDS and FireFOAM make use of the LES turbulence approach while ISIS employs the Reynolds-Averaged-Navier-Stokes (RANS) equations with the k-epsilon turbulence model. FireFOAM and FDS have different turbulence models but the default model for FireFOAM is the one equation eddy viscosity model, while FDS makes use of the modified Deardorff model. The standard FireFOAM, FDS and ISIS use the fast chemistry approach for combustion. The mean reaction rate is modelled using the Eddy Break-Up Model for ISIS, while FDS and FireFOAM employ the Eddy Dissipation Concept.

2.1. Conjugate heat transfer (CHT)

Eqs. (1)-(3) represent the equations for the fluid region. In the solid region, only the energy equation, which is given as:

$$\frac{\partial(\bar{\rho}h)}{\partial t} = \nabla.(\lambda_s \nabla T) + Q \qquad (5)$$

is considered. The solid regions in the present study, based on the PRISME experimental scenarios, are concrete and rock wool while the fluid region is the gas phase where combustion takes place. CHT allows for coupling the thermal energy transport between the

fluid and solid region. Using Eq. (5) CHT is implemented as a 3D model in FireFOAM. The present study couples the CHT solver to the combustion process to represent accurately the heat transfer process in the walls of the fire compartment. The CHT libraries are linked together with the combustion libraries present in the open-source CFD-toolbox OpenFOAM to allow for heat transfer and combustion processes to run simultaneously. The heat transfer between solid and fluid, as a result of their interaction is stated mathematically using CHT. To solve CHT problems, the continuity of both temperature and heat flux at the interface of the fluid and solid region need to be ensured using the following two conditions:

$$T_f = T_s \tag{6}$$

$$\lambda_f \frac{\partial T_f}{\partial y}\Big|_{y=+0} = \lambda_s \frac{\partial T_s}{\partial y}\Big|_{y=-0} \tag{7}$$

where the subscripts f and s are for fluid and solid respectively. The local coordinate normal to the solid is denoted as y. The three modes of heat transfer, convection, radiation and conduction are solved using the CHT solver. Convective heat transfer at the walls is derived using wall functions that make use of universal behaviour of the flow near the wall (Versteeg and Malalasekera, 2007). The wall functions allow for the prediction of the gradients of velocity and temperature at the cells adjacent to the wall interface boundary assuming a fully developed boundary layer. Thermal conduction from solid cell to wall boundary is given as:

$$q = \frac{\lambda_s}{\Delta n}(T_w - T_s) \tag{8}$$

where λ_s is the thermal conductivity and T_s the temperature of the solid. Δn represents the distance between the surface of the wall and the centre of the solid cell. The condition at the interface for the radiative heat transfer is given as (McGrattan et al., 2003):

- from fluid to solid

$$\lambda_{eff} \frac{\partial T_f}{\partial y}\Big|_{y=+0} + q_{rad,in} = \lambda_s \frac{\partial T_s}{\partial y}\Big|_{y=-0} \tag{9}$$

- from solid to fluid

$$\lambda_{eff} \frac{\partial T_f}{\partial y}\Big|_{y=+0} = \lambda_s \frac{\partial T_s}{\partial y}\Big|_{y=-0} - q_{rad,out} \tag{10}$$

where λ_{eff} is the effective conductivity, $q_{rad,in}$ is the incident radiative heat flux going into the solid given as:

$$q_{rad,in} = \int_{\vec{n}.\vec{s}<0} I_s(\vec{s}) |\vec{n}.\vec{s}| d\Omega \quad (11)$$

and $q_{rad,out}$ is the radiative heat flux leaving the solid, expressed as:

$$q_{rad,out} = \frac{1}{\pi}\left[\kappa_s \sigma T_s^4 + (1 - \kappa_s) q_{rad,in}\right] \quad (12)$$

where κ_s is the absorptivity of the solid.

The current method of performing CHT is the iterative method in which the fluid and solid equations are solved separately. The fluid domain is solved first with an initial guess of the temperature at the interface. The heat flux obtained from the fluid domain is used to solve the energy transport in the solid domain to obtain the new value for temperature and so on. This process continues until convergence is achieved with the desired accuracy. The iteration process relies on the idea that each domain provides a boundary condition for the other at the interface.

CHT as mentioned earlier would be used to represent the heat transfer in the walls for the current study. Previous studies using FDS and ISIS solved heat transfer in the walls using the 1D Fourier equation for conduction and standard wall laws for the convective flux. The wall laws relied on establishing empirical correlations for the heat transfer coefficients. CHT would therefore allow for a more realistic representation of heat transfer at the walls and a wider range of applications without having to adjust the empirical correlations.

2.2. Mechanical Ventilation Model

The 1D ventilation model implemented in the present study in the in-house FireFOAM version is based on a generalized Bernoulli Equation. It also includes source terms accounting for buoyancy effects, transient conditions, and energy. The model solves for the mass and momentum equation in the mechanical ventilation domain which is given as:

$$\frac{\partial \rho}{\partial t} + \frac{\partial \rho u}{\partial x} = 0 \quad (13)$$

$$\rho \frac{\partial u}{\partial t} + \rho u \frac{\partial u}{\partial x} = -\frac{\partial p}{\partial x} + \sum S \quad (14)$$

where u is the longitudinal velocity, ρ is the fluid density and S is the longitudinal source term. The static pressure is represented by p while x and t represent the longitudinal and temporal coordinates respectively. The source term contains terms like buoyancy, wall friction and pressure due to fan operations.

The ventilation domain is discretized into control volumes and the 1D problem is solved. The control volume contains nodes denoted as i and branches denoted as j. A node contains the

field variables and properties of the fluid such as temperature, pressure, mass, molar fractions etc. A branch contains geometric and thermal properties such as length, area, roughness, and wall temperature. A branch also connects two nodes. In the case of a nuclear compartment, a node represents location where a duct connects to the computational domain or where multiple ducts join. An example of the network representation is given in Fig. 1.

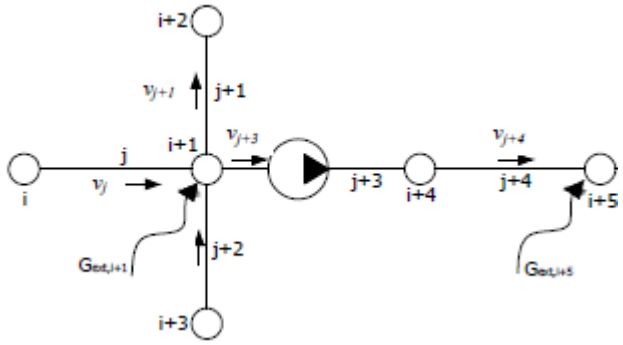

Fig. 1. A network representation of a ventilation duct showing branches between nodes (Colella, 2010).

The present study deals with the steady-state equation and the integration of the mass and momentum is given as:

$$\sum_j \rho_j u_j A_j = 0 \tag{15}$$

where A is the area of the branch. Eq. (15) shows that the sum of the mass flow rates entering a node must be equal to the mass flow rate exiting the node.

$$(P_i - P_{i-1}) + \Delta P_{FAN,j} - \frac{1}{2} K \rho_j u_j^2 + (\rho g \Delta z)_j = 0 \tag{16}$$

where K is the total flow loss or loss coefficient and includes pressure losses due to friction and fitting losses in the ventilation ducts. Eq. (16) is derived from the integration of Eq. (14) along a ventilation branch, j from node i to $i-1$. Ignoring the time derivatives leads to the steady-state in Eq. (16). The total flow loss with an already determined duct roughness is given as:

$$K = \frac{fL}{D} \tag{17}$$

Where f is the friction factor, L is the duct length and D is the diameter of the duct. The friction factor is obtained by an approximation developed by Zigrang and Sylvester (1982):

$$\frac{1}{\sqrt{f}} = -2\log_{10}\left(\frac{\frac{\varepsilon}{D}}{3.7} - \frac{4.518}{Re_D}\log_{10}\left(\frac{6.9}{Re_D} + \left(\frac{\frac{\varepsilon}{D}}{3.7}\right)^{1.11}\right)\right) \tag{18}$$

where ε is the absolute roughness of the duct, D is the diameter of the duct and Re_D is the Reynolds number of the flow in the duct. The value for the absolute roughness of the duct is based on the duct material. The flow loss is derived and is included in the momentum equation for the duct flow.

The pressure rise due to fans, $\Delta P_{FAN,j}$ is usually represented as a generic polynomial of second order. The curve is known as the fan characteristic curve with curve coefficients a, b and c as:

$$\Delta P_{FAN,j} = a + bu_j + cu_j{}^2 \quad (19)$$

The curve coefficients are obtained from empirical correlations. The pressure rise from the fans is not considered in this study because there were no fans present in the experimental set-up. There was no elevation therefore $(\rho g \Delta z)_j$ was also not considered in this study. Eq. (16) is therefore reduced to a simplified Bernoulli Equation like FDS and ISIS which is given as:

$$(P_i - P_{i-1}) - \frac{1}{2} K \rho_j u_j^2 = 0 \quad (20)$$

The SIMPLE Algorithm is used to solve the continuity and momentum equations for both steady and transient problems.

The mechanical ventilation model in the present study needs to be coupled to the 3D flow field like the ventilation model in FDS. The solution procedure however differs, and this mostly includes the difference in solving for pressure in the compartment that would be coupled to the discretized momentum equation of the ventilation model. Further discussion on the pressure solution is beyond the scope of this work and the reader could find more details in McGrattan et al. (2015). ISIS makes use of a simplified Bernoulli formulation which is applied as a boundary condition at the inlet and outlet ventilation branch. The Bernoulli formulation is supplemented by a mass balance equation containing the flow rates of the ventilation branch and pressure of the compartment. The mass balance equation ensures total mass conservation of the compartment. The use of a more advanced Bernoulli equation is important when looking into complex set-ups like a multiple rooms configuration with a ventilation system going across multiple rooms. In the present study, the experimental set-up simplifies the current ventilation model as shown in Eq. (20).

2.2.1 Coupling 1D Ventilation Model and 3D Room flow field

In the present study, the inlet and outlet ventilation ducts are represented as one branch with nodes at both ends with one of the nodes located at the interface between the 1D ventilation model and 3D room flow field model. To ensure continuity, at the interface denoted as a, it is assumed that:

Area A(a^-) = A(a^+) (21)

Mean pressure $\bar{p}(a^-) = \bar{p}(a^+)$ (22)

Mean velocity $\bar{v}(a^-) = \bar{v}(a^+)$ (23)

The 1D ventilation duct provides the average values for the fluid-dynamic quantities shown above which are used at the boundary faces of the 3D domain. To provide values to the 1D ducts, the fluid-dynamic quantities are reduced to single values by averaging at the 3D faces:

$$\bar{u}(a^-) = \frac{1}{|\Gamma_a|}\int_{\Gamma_a} u \,.\, n \, d\sigma \quad (24)$$

$$\bar{p}(a^-) = \frac{1}{|\Gamma_a|}\int_{\Gamma_a} p \; d\sigma \quad (25)$$

$$\dot{m}(a^-) = \int_{\Gamma_a} \rho u \,.\, n \, d\sigma \quad (26)$$

Where p is the pressure, u represents the velocity, ρ represents the density and n is the vector normal to the interface Γ_a.

As mentioned earlier, the 1D model would be represented by a single branch with two nodes at the end. The 1D ventilation model and 3D flow field model would be solved separately during the iterative process. The node which is not connected to the 3D compartment would have a fixed value for pressure, while the node connected to the 3D compartment would derive the pressure value from the 3D flow field model. The following procedure is followed:

- The process starts with the 3D model providing pressure value to the 1D ventilation model.
- The 1D ventilation model uses the new pressure value to calculate the velocity values which would be used as the boundary condition for the 3D model.
- The new velocity value at the boundary faces is used to get new pressure values for the 3D model which would, in turn, be used as a boundary condition for the 1D model.
- The process repeats itself ensuring that the pressure values are obtained for the 3D model and the velocity values are found at the 1D domain during the fire occurrence.

The coupling of the 3D model and 1D ventilation takes place every time step and internal ventilation. Numerical tolerance set for the simulation is given as 10^{-6} (Colella, 2010).

3. Experimental Scenario for model verification and validation

The experimental data used to validate the ventilation model implemented into the in-house FireFOAM were obtained during PRISME Source campaign of the PRISME 1 project in the IRSN DIVA facility within a large-scale compartment with a volume of 3600m^3 known as JUPITER (Audouin et al., 2013). The DIVA facility consists of three rooms with a volume of 120m^3 ($5m \times 4m \times 6m$) located at the bottom, one 170m^3 room at the top and a corridor with a volume of 150m^3 connecting the three rooms at the bottom. A mechanical ventilated network connects all the rooms. The facility can withstand a gas pressure range of 10kPa to 52kPa.

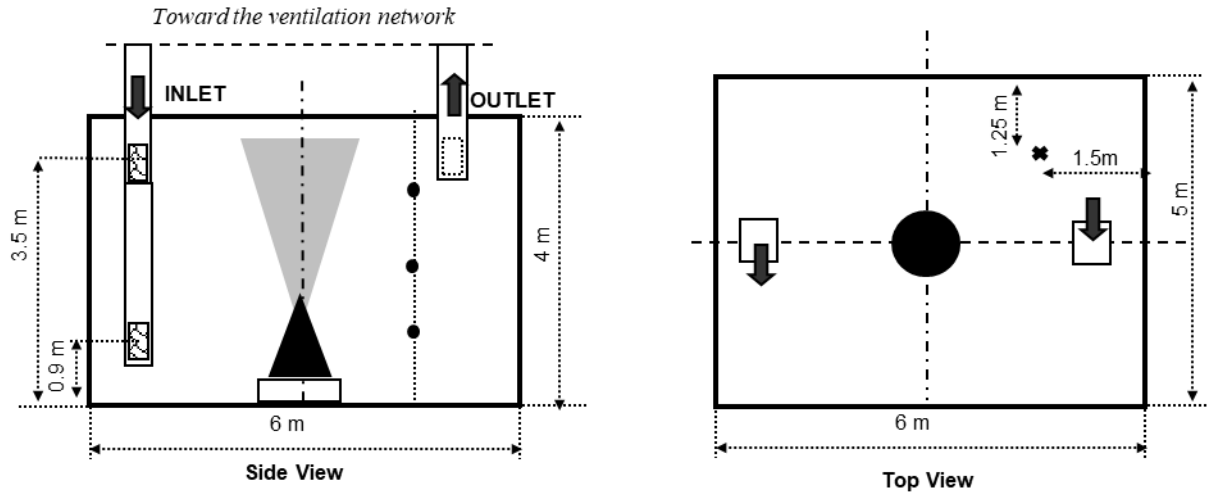

(a) (b)

Fig. 2. (a) East wall side view and (b) Top view of the fire room; the two positions of the inlet branch are indicated (Audouin et al., 2013)

In the present study, only single room fire tests are considered. The room has an actual volume of 118.5m^2 and a 30cm thick reinforced concrete. Fig. 2 shows the side and top view of the room including the position of the ventilation networks. The ceiling is insulated with 5cm panels of thick rock wool. The thermal properties of concrete and rock wool are given in Table 1.

Table 1. Wall properties in the compartment (Audouin et al., 2013)

Material	**Heat**	**Heat Capacity**	**Emissivity ε**	**Density**

	Conductivity $\boldsymbol{k}$ **(W**$\mathbf{m^{-}K^{-1}}$)	$\boldsymbol{Cp}$ $(\mathbf{Jkg^{-1}K^{-1}})$		$\boldsymbol{\rho}$ $(\mathbf{kgm^{-3}})$
Concrete	1.5	736	0.7	2430
Rock wool	0.012	840	0.95	140

The room is mechanically ventilated and closed. The ventilation is made with two branches (one inlet and one exhaust). The inlet branch can be set at two locations, in the upper part or the lower part of the room as illustrated in Fig. 2. The exhaust branch is always positioned in the upper part of the room. The two branches are connected to an industrial ventilation network consisting of one blowing line and one exhaust line both equipped with fans and dilution lines. The branches inside the room consist of rectangular ducts with a cross-section of 0.18m^2 (0.3m x 0.6m) entering the rooms. The density of air is assumed to be 1.18 kg/m^3.

In the present study, four tests of the PRISME Source campaigns have been considered. The choice of the tests was based on past similar studies with FDS and ISIS. The use of four tests was also motivated by the fact that all three tests had the same experimental set-up, with the difference being the initial ventilation flow rate and pressure. The fourth test had a longer inlet closer to the fuel and a different ventilation flow rate. The results would be sufficient to study the ventilation model. Table 3 presents the values of the main parameters of the tests with the air renewal rate and ventilation position.

For the four tests, the fire is a circular pool fire positioned at the centre on the room. The pool is filled before ignition with 14.6 kg of hydrogenated tetra-propylene (TPH). The fuel is treated as dodecane ($C_{12}H_{26}$) with the following stoichiometric chemical reaction:

$C_{12}H_{26} + 18.5O_2 + 69.6N_2 \rightarrow 12CO_2 + 13H_2O + 69.6N_2$

The properties of the fuel are shown in Table 2.

Table 2. Fuel properties. (Audouin et al., 2013)

Heat of Combustion, $\Delta \boldsymbol{H_c}$ **(J/kg)**	4.2×10^7
Heat of gasification (kj/kg)	361
Molar mass	$0.17 kg/m^3$
Lower Oxygen limit	10%

Total mass	14.6 kg
Density ρ $(\mathbf{kgm^{-3}})$	749
Boiling point (K)	461

The fuel tank is 10cm deep and made of carbon steel that is 5mm thick. The fuel tank is placed on a scale located 0.4m above the floor. The area of the pool surface is 0.4m^2.

Different fuel mass loss rate (MLR) and thus different Heat Release Rate values have been measured due to the changes in the ventilation conditions. As mentioned in the introduction, these tests have been already simulated with ISIS code (Nasr et al., 2011; Suard et al., 2013; Perez et al., 2017; Suard et al., 2011; Audouin et al., 2011) and with FDS code (Wahlqvist and Hees, 2016; Sikanen and Hostikka, 2017). The physical phenomena observed during these tests have been discussed by Prétrel et al. (2005), Le Saux et al. (2005) and Prétrel et al. (2012).

Measurements that will be compared with the simulations results are the static pressure in the room and the volume flow rates measured in each ventilation branches. The data have been collected from (IRSN, 2013).

Table 3. Test conditions for the PRISME Source experiments considered in the present study.

Test	**Flow in and out (m^3/h)**	**Position of inlet**
PRS_SI_D1 (or PRSID1)	560	High
PRS_SI_D2 (or PRSID2)	1020	High
PRS_SI_D3 (or PRSID3)	180	High
PRS_SI_D6a (or PRSID6a)	200	Low

4. Initial and Boundary Conditions for simulations

Table 4 shows the values for the initial conditions of each four fire tests, and Table 5 presents the pressure and loss coefficients for each of the four fire tests.

Table 4. Initial condition for the four fire Tests.

Variable	**Initial condition**
Velocity	(0.0 0.0 0.0) m/s
Temperature (Gas and Wall)	307 K
Pressure	98384 Pa

Turbulent kinetic energy	$1.0 \times \frac{10^{-6}\, m^2}{s^2}$
Mixture fraction	0.0
Fuel mass fraction	0.0

Table 5. Pressure and loss coefficients at Ventilation Branch.

Test	**Inlet Pressure (Pa)**	**Outlet Pressure (Pa)**	**Inlet Loss Coefficient**	**Outlet Loss Coefficient**
PRS_SI_D1	98413	97536	164.04	1694.82
PRS_SI_D2	98419	97649	25.47	484.81
PRS_SI_D3	98570	97624	3001.77	12623.59
PRS_SI_D6a	98499	97674	2046.16	12632.78

The inlet and outlet loss coefficients are calculated from Eq. (20)**.** P_i and P_{i-1} represent the initial pressure in the compartment and Inlet/Outlet pressure in the ventilation respectively, while ρ and u represent the density and velocity respectively in the compartment. The pressure, density and velocity values used for calculating the loss coefficients are derived at steady state before ignition. Rewriting Eq. (20), the loss coefficient is calculated using the formula $K = \frac{2(P_i - P_{i-1})}{\rho_j u_j^2}$ which can also be expressed as $K = \frac{2\,\Delta \mathrm{p}}{\rho u^2}$.

A cartesian hexahedral mesh that covers the whole domain is used in the simulations. The size of the mesh is determined using a grid sensitivity study that would be discussed in a different section below.

At the inlet and outlet of the ventilation branch, the mechanical ventilation model is coupled with the in-house FireFOAM where pressure and velocity values would be exchanged. The pressure at the inlet and outlet of the ventilation branch is set for each test prior to ignition. The mechanical ventilation model supplies the inlet and outlet velocity at the ventilation branches.

The turbulent kinetic energy is set at the outlet and inlet using the branch velocity, turbulent intensity and dissipation rate. The turbulent intensity is 0.01 and the mixing length scale is set to 0.03m (Bonte et al., 2013).

At the fuel inlet, the experimental mass flow rate is used to calculate the velocity. The simulations are performed without modelling the burning rate but using the experimental measurements of the mass loss rate given in Fig.3.

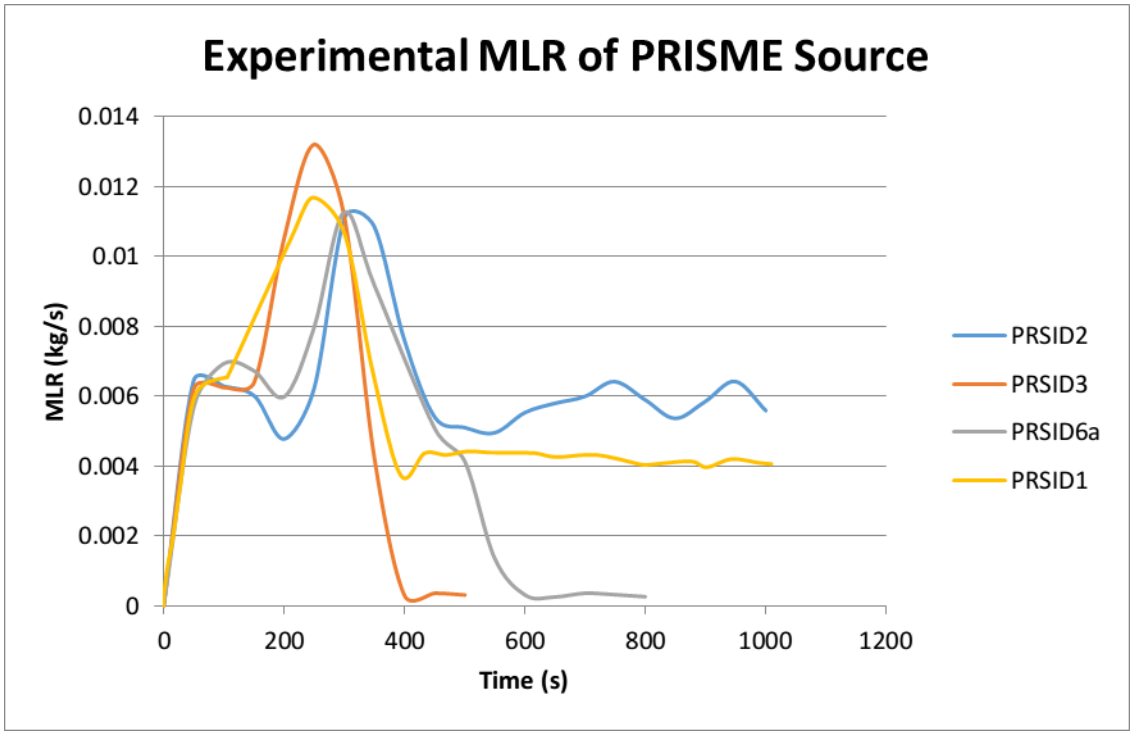

Fig. 3. Experimental Mass Loss Rate (MLR) of each four fire tests (only the first 1000s of the tests are presented for test PRSID1 and PRSID2).

A diffusive radiation condition is used for the radiative intensity with emissivity set to 1. The pool wall is assumed to be adiabatic.

At the interface between the fluid and solid, a mixed boundary condition is set for temperature and radiation heat transfer. The mixed boundary condition is a combination of a fixed value and fixed Gradient boundary condition. This means that the boundary condition can switch between two boundary conditions using a weighting process. The heat transfer between the concrete walls and Rock wool ceiling are also calculated using the mixed boundary condition for temperature and radiation. Boundary conditions at the exterior are assumed to be adiabatic including the ventilation inlet and outlet.

A zero gradient boundary condition is used for the species and pressure. No-slip boundary condition is applied to the walls.

5. Results and Discussion

This section presents the simulation results obtained using the newly modified version of FireFOAM with the implemented ventilation model and CHT. These results are compared to the experimental results and are mainly concerned with the analysis of pressure variations

and flows at the inlets and outlets, and characterizing the behaviour of the ventilation system.

5.1. Grid Sensitivity study

A grid sensitivity analysis was first carried out to determine the appropriate optimum grid size, PRS_SI_D1 was chosen as a representative test. The grid size was studied based on previous works of Sikanen and Hostikka (2017), McGrattan et al. (2003) and Lin et al. (2009). They rely on the concept of the ratio of the hydraulic diameter to the grid size, $\frac{D^*}{\delta x}$ where D^* is the characteristic fire diameter, expressed as:

$$D^* = \left(\frac{\dot{Q}}{\rho_\infty C p T_\infty \sqrt{g}}\right)^{\frac{2}{5}} \quad (27)$$

where $\dot{Q}$ is the total Heat Release Rate (HRR). The minimum value of HRR is approximately 4900 W and the maximum value is 130000 W. The ratio, $\frac{D^*}{\delta x}$ is the number of cells spanning the fire. Various studies have come up with an adequate resolution based on the ratio and the limitations of computational speed. Sikanen and Hostikka (2017) did a grid sensitivity study using ISIS for PRSID1 but it was mainly focused on the MLR at the fuel inlet. The current study would focus on the entire domain and would be concerned with the pressure and flow rate at the inlet ventilation branch. The values for $\frac{D^*}{\delta x}$ for 100mm, 60mm, 27mm is given as 10, 20 and 41 respectively. Three meshes with hexahedral cell numbers of 153280, 280000 and 518570 are used for the grid sensitivity study. To avoid convergence problems, the mesh size is applied all over the domain including the ventilation branches. The mesh sizes are divided into coarse, medium, and fine meshes. The ratio for the different mesh sizes is 6, 8 and 12 respectively. The mesh sensitivity study was performed for PRS_SI_D1 tests and Fig. 4 shows the different study for pressure.

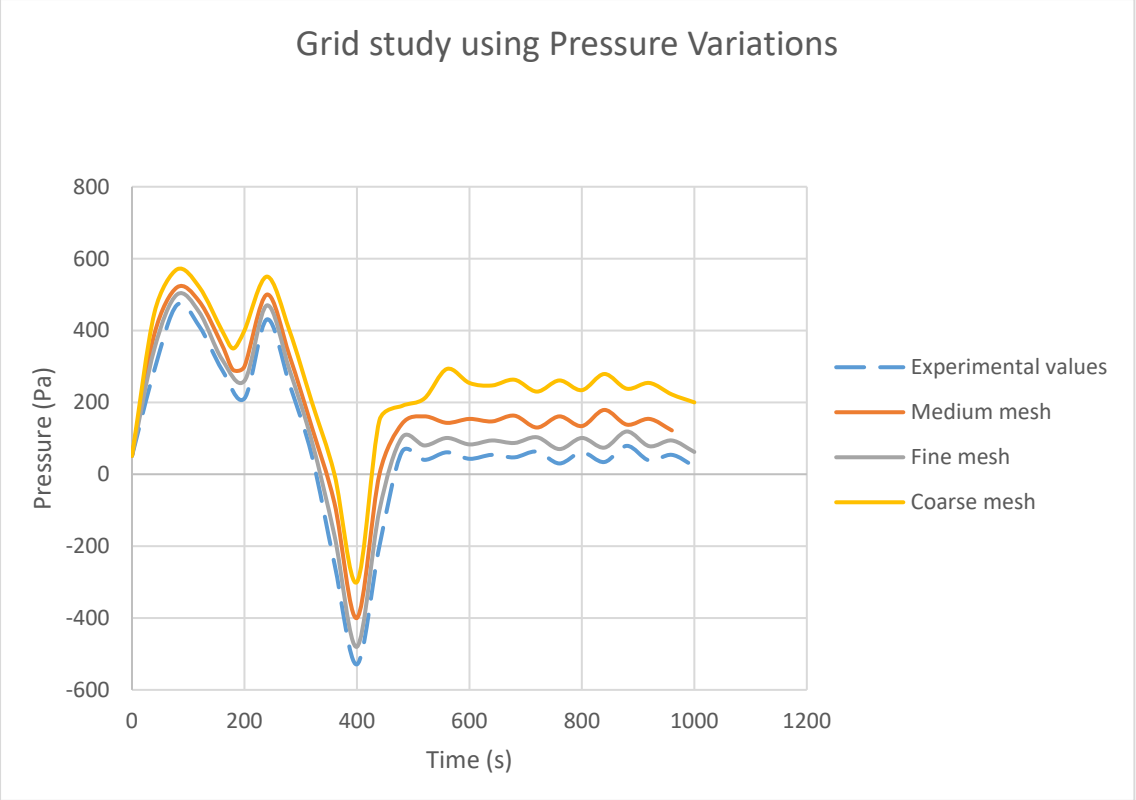

Fig 4. Grid study for pressure variations inside a fire compartment (1000 first seconds of test PRS_SI_D1).

Fig. 4 shows the pressure variation with the pressure peak for both experimental and simulated values of the different grid size. The data points chosen for Fig. 4 capture the pressure peaks when compared to the experimental values from the original data. The medium and fine meshes have very close values with a percentage difference of approximately 6%. The fine mesh took approximately double the time to run when compared to the medium mesh. The computational time for the simulations were 70,840 seconds for coarse mesh, 111,600 seconds for the medium mesh and 218,118 seconds for the fine mesh on 25 CPUs in parallel. The medium mesh was selected because it is an acceptable compromise between accuracy and computational time.

5.2 Non-reacting results

The first 60s of the simulation is run without combustion to get the steady ambient conditions of the pressure and flow rate before the fire is ignited. This process is important to confirm that before ignition, the simulation matches the equivalent pre-combustion

experimental results. The modified in-house version of FireFOAM was used to simulate the non-reacting process and the results are shown hereafter.

Figs. 5 and 6 show that experimental and simulated results are overall in good agreement with each other. A percentage difference of approximately 2% is found and this means that the ventilation model can be used for the fire scenario stage.

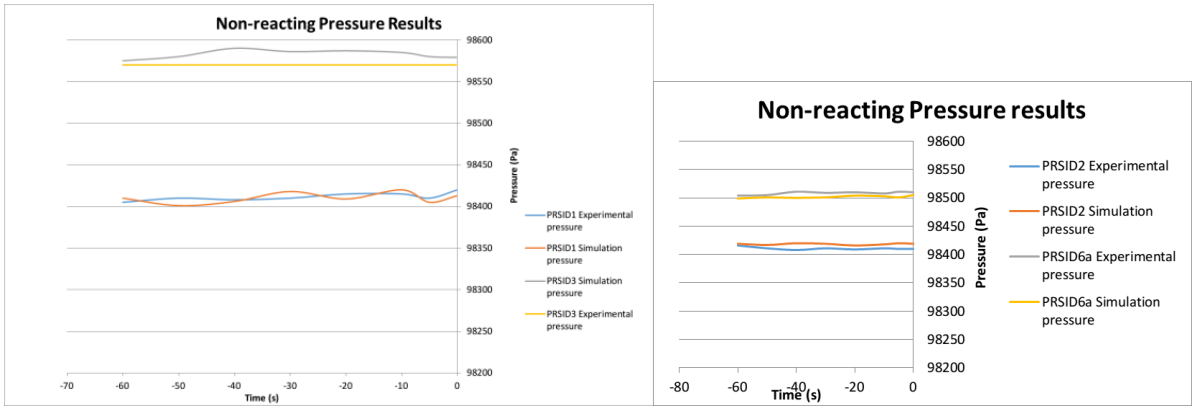

Fig. 5. Pre-combustion pressure results in the compartment.

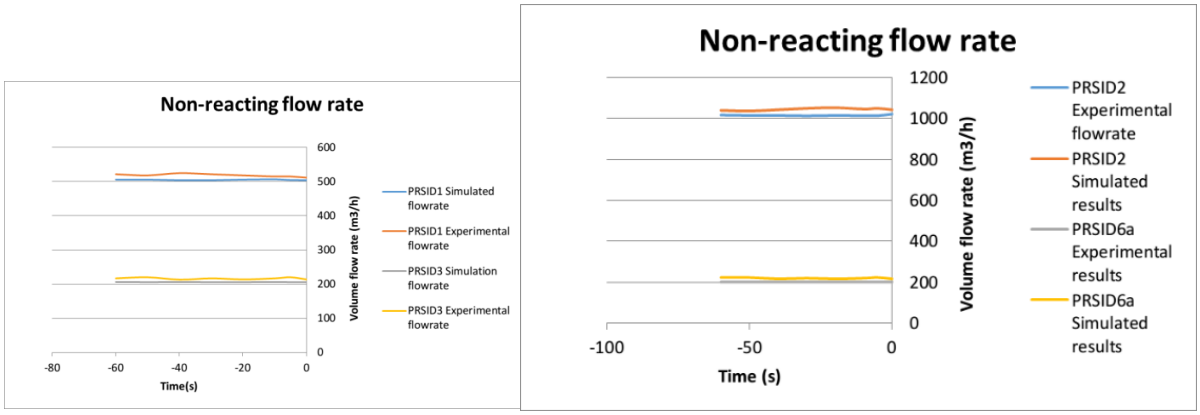

Fig. 6. Pre-combustion flow rate results in the ventilation branch.

5.3. Pressure Variations inside Fire Compartment

The simulation results for PRSID1, PRSID2 and PRSID6a do not show the extinction phase of the fire and terminate at the steady phase. The reason for not including the extinction phase was mainly due to limited computational resources and long computational times. The results for PRSID3 contain the entire phase of the fire which makes it possible to study the pressure variations and the mechanical ventilation model. The results from PRSID3 therefore provide an acceptable reason to neglect the extinction phase of the other test

studies and focus on the ignition and unsteady phase. Before ignition, the first 60s of the simulation was run without combustion to match the pre-ignition experimental results.

As shown in Figs. 7-10, the mechanical ventilation model predicts the pressure variations inside the fire compartment with an acceptable level of accuracy. The pressure variations including the experimental and predicted pressure values depict the expected behaviour which includes an unsteady period with an overpressure peak at ignition, a long quasi-steady period with other peaks during combustion, another unsteady period with an under-pressure peak as a result of a sudden decrease of MLR, and a steady-state stage with slight fluctuations. The overpressure peak leading to flow inversion at the admission line is due to the gas expansion that causes uncontrolled behaviour in the ventilation branches. It can also be seen from Figs. 7 to 10 that the mechanical ventilation model can capture the two overpressure peaks at ignition which are caused by the chemical reaction releasing energy and quick changes in the heat release rate of the fire. The flow rate at the stationary stage is also well predicted. The negative pressure is due to heat losses through the walls and vents being larger than the heat generated by the fire. This leads to a peak in the inlet ventilation flow rate and an increase in the oxygen concentration which would increase the heat from the fire and reverses the negative pressure.

Fig. 10 showing the pressure variation for the low inlet position contains two under-pressure peaks during the decrease of MLR while the other experiments with high inlet position have one under-pressure peak. This shows the importance of the ventilation configuration because, at the low position, oxygen is supplied closer to the fuel source affecting the burning rate of the fuel.

From the description of the pressure variation behaviour, it is shown that the pressure variation and the ventilation flow rate are linked to the fuel MLR. Fig. 3 contains the MLR for the different PRISME Source tests. From Fig. 3 the increase in MLR at the initial stages leads to an increase in the pressure which affects the flow rate. The reduction in the flow rate leads to a decrease in MLR and pressure. The flow rate increases again and the MLR and pressure increases. A steady phase is reached with the MLR during the combustion process. During the extinction phase for PRSID3, there is an increase in the pressure and flow rate. The coupling process between the MLR, pressure and flow rate are depicted in the plotted graphs.

In Figs. 7 to 10 the overpressure peak is slightly under-predicted meaning that the inlet ventilation branch starts to reverse under less pressure which can be seen from Figs. 11 to 14. The inlet ventilation branch performs the function of a pressure relief which means that at the reverse stage, the predicted pressure is lower.

PRS_SI_D6a contains the results with the highest difference between the experimental and predicted values as shown in Fig. 10. It is worth noting that similar differences were reported for the same test by Wahlqvist and Van Hees (2013) using a different CFD code (FDS). Wahlqvist and Van Hees (2013) suggested that the large differences could be the result of some inconsistencies in the calculation of loss coefficient or some unreported changes in the system during the experiments. They came to this conclusion as a result of the good agreements between the experiment and predicted temperatures inside the fire compartments for both tests. The predicted and numerical temperature results according to Wahlqvist and Van Hees (2013) also suggest that the issue is isolated to the PRS_SI_D6a experiment. Fig. 20 shows the good agreements between predicted and experimental temperatures.

The other cases have relatively lower differences between the experimental and predicted values and within the experimental uncertainty of 30% (Audouin et al., 2011).

The calculation of the loss coefficients as mentioned above could also include discrepancies in experimental data which would affect the predictions. The value of the loss coefficient is also kept constant throughout the simulation. To understand the effect of the discrepancies due to loss coefficients, a sensitivity study should be performed. Such a sensitivity study of the loss coefficients has been previously performed in Bonte et al. (2013) in which the authors reported that an uncertainty of ±10% on the loss coefficients is acceptable for performing simulation. Bonte et al. (2013) also highlighted that the loss coefficients have the largest influence on pressure results. To understand further possible discrepancies, the oxygen concentration and gas temperatures are presented in the following sections. Like the over-pressure peak, the under-pressure peak is also slightly under predicted.

Fig. 7. Pressure variations inside the nuclear compartment -Predictions vs Experimental data (1000 first seconds of test-PRS_SI_D1).

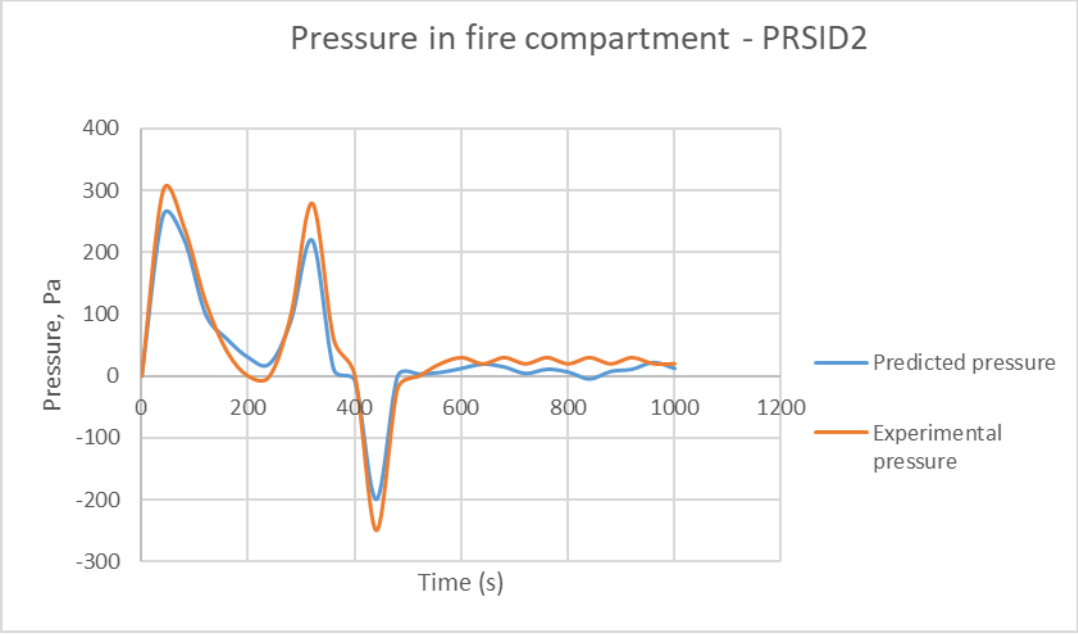

Fig. 8. Pressure variations inside the nuclear compartment -Predictions vs Experimental data (1000 first seconds of test-PRS_SI_D2).

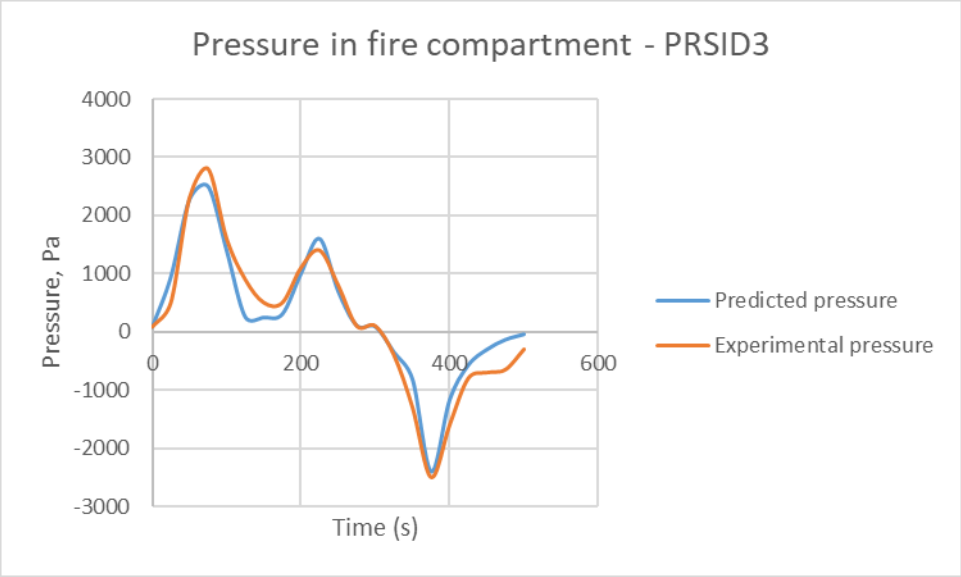

Fig. 9. Pressure variations in the nuclear compartment -Predictions vs Experimental data (PRS_SI_D3).

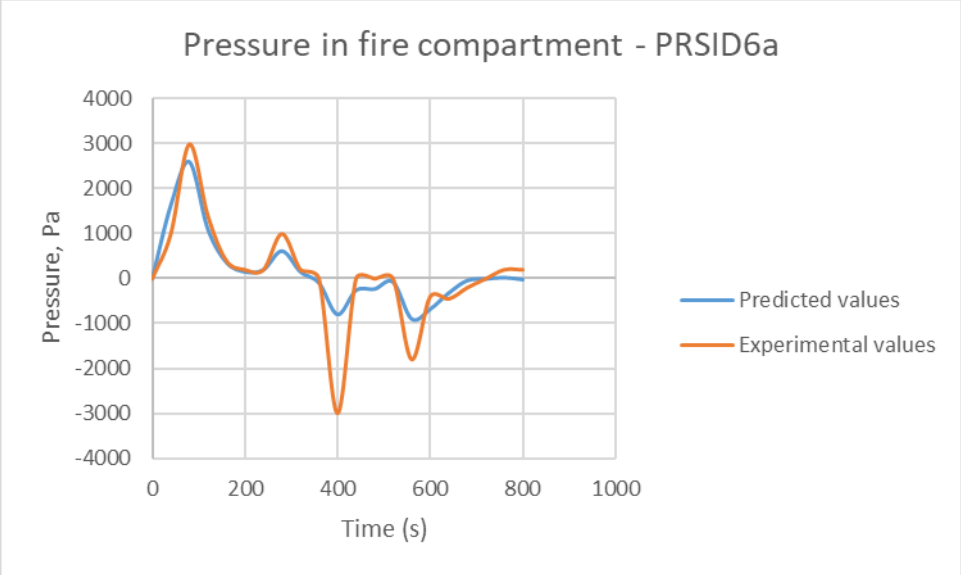

Fig. 10. Pressure variations in the nuclear compartment -Predictions vs Experimental data (800 first seconds of test-PRS_SI_D6a).

5.4. Volume flow rate at Inlet Ventilation Branch

The overpressure peak causes a decrease of flow at the inlet ventilation branch which could lead to a flow inversion. The under-pressure peak leads to an increase in the flow at the inlet ventilation branch which could cause backflow into the nuclear compartment. This behaviour can be seen from Figs. 11-14. Flow inversion is noticed when the overpressure peak is greater than the pressure at the inlet.

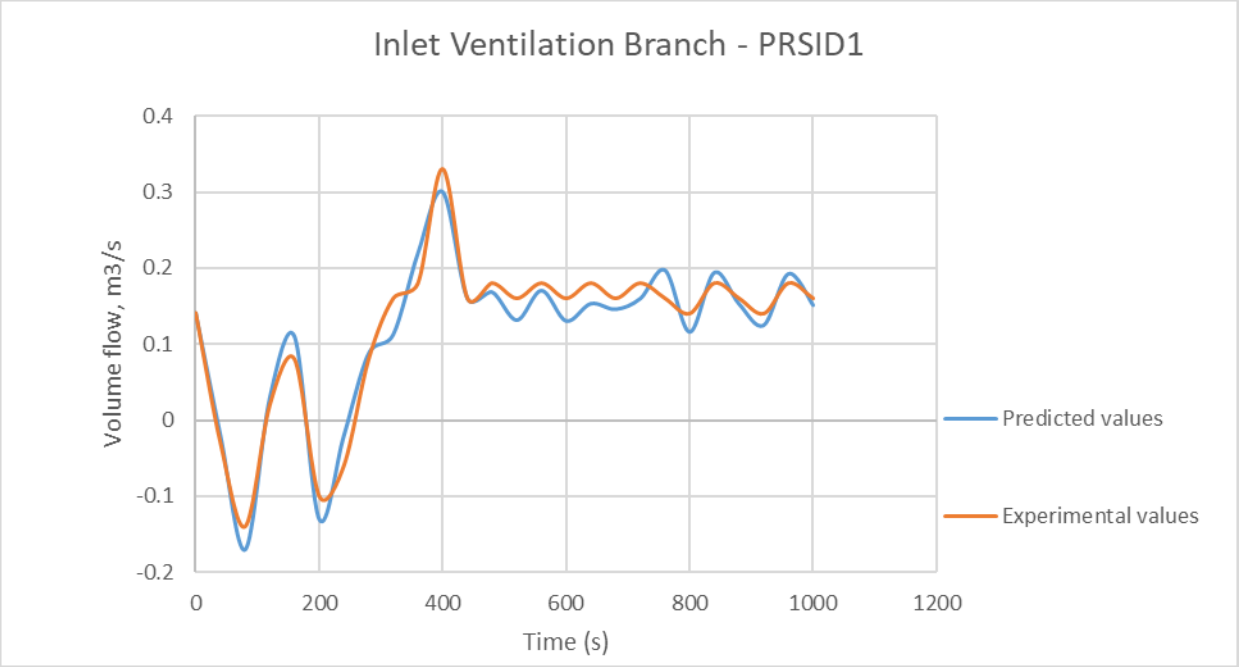

Fig. 11. Volume flow rate at the inlet of ventilation branch – Predictions vs experimental data (1000 first seconds of test-PRS_SI_D1).

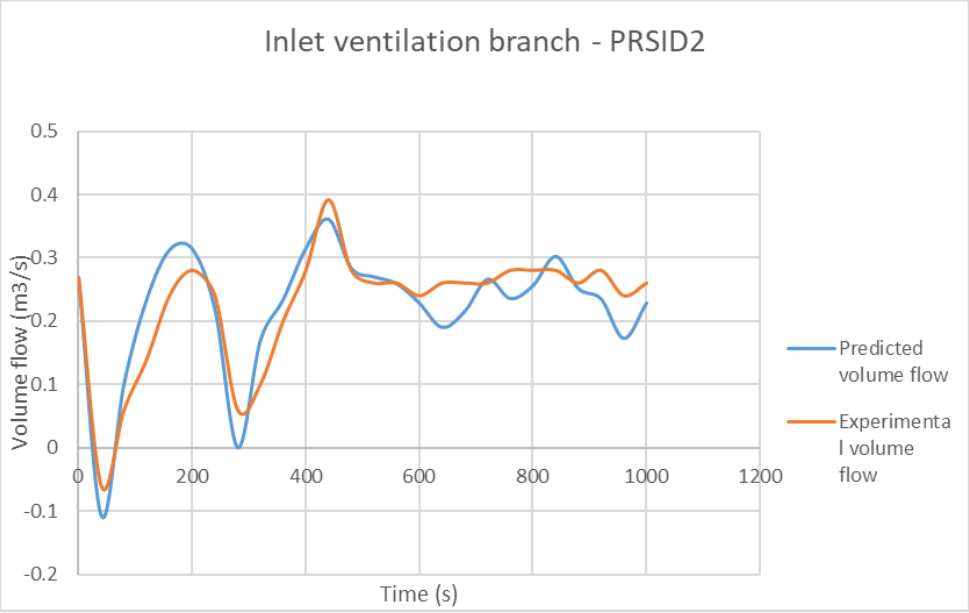

Fig. 12. Volume flow rate at the inlet of ventilation branch – Predictions vs experimental data (1000 first seconds of test-PRS_SI_D2).

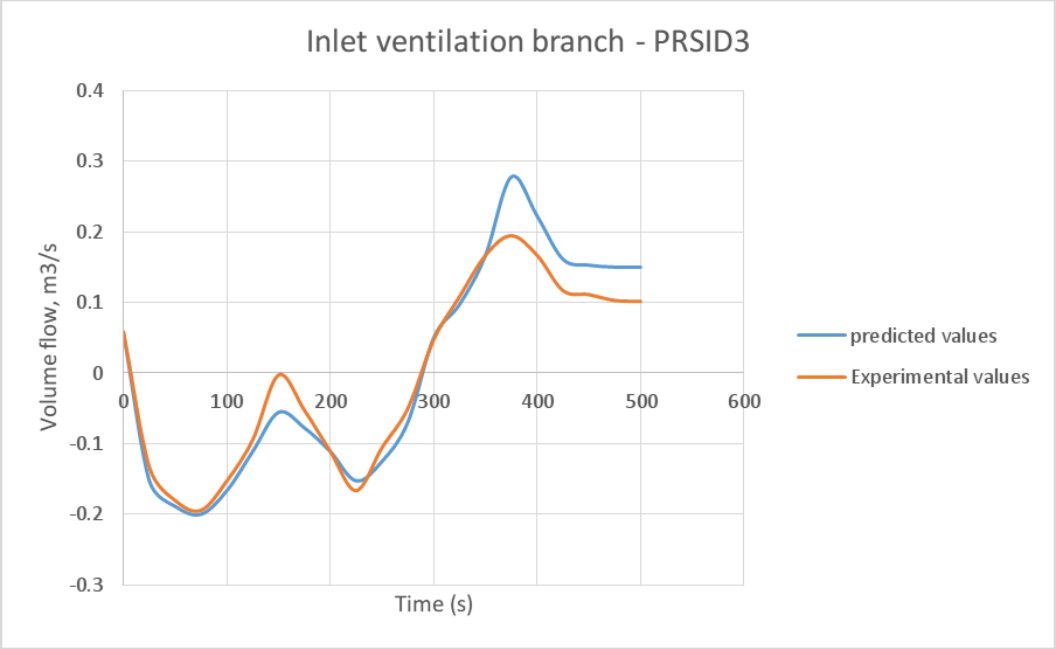

Fig. 13. Volume flow rate at the inlet of ventilation branch – Predictions vs experimental data (PRS_SI_D3).

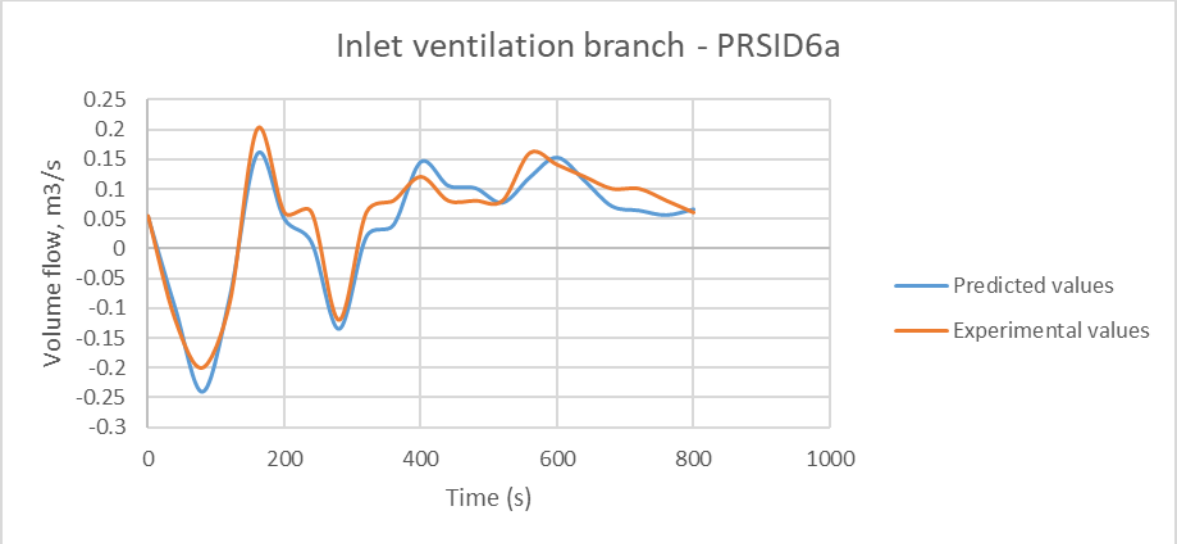

Fig. 14. Volume flow rate at the inlet of ventilation branch – Predictions vs experimental data (800 first seconds of test-PRS_SI_D6a).

5.5. Volume flow rate at Outlet Ventilation Branch

The overpressure peak on the other hand causes a slight increase in the outlet ventilation branch. During the under-pressure peak, the flow at the outlet ventilation branch decreases. Reverse flow occurs when the pressure at the outlet is greater than the under-pressure peak. This behaviour can be seen in Figs. 15-18.

Comparing the behaviour of the inlet ventilation branch and Outlet ventilation branch for the different tests, it is shown that flow at the inlet is more sensitive to the pressure variation than outlet flow. This behaviour is expected because the outlet branch is more resistive than the inlet one. From Table 5 the loss coefficients for the outlets are higher than the inlets ones which is due to the tuning of the valves in the ventilation branch. The higher values of the outlets mean that the outlet branch would have less pressure and flow rate variations compared to the inlet.

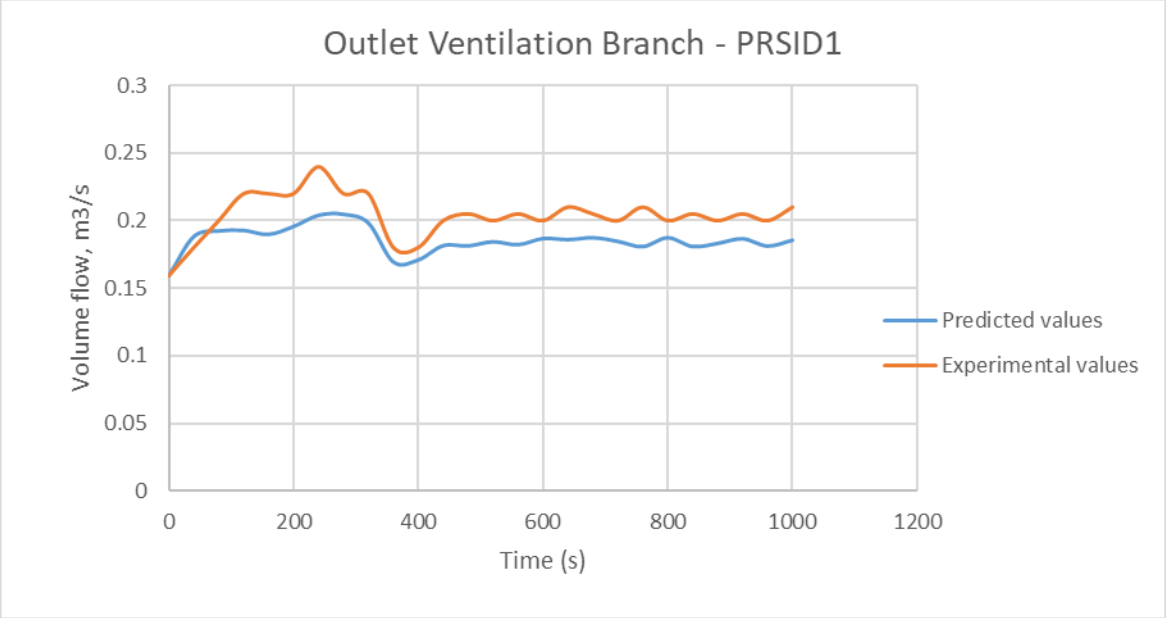

Fig. 15. Volume flow rate at outlet of ventilation branch – Predictions vs experimental data (1000 first seconds of test-PRS_SI_D1).

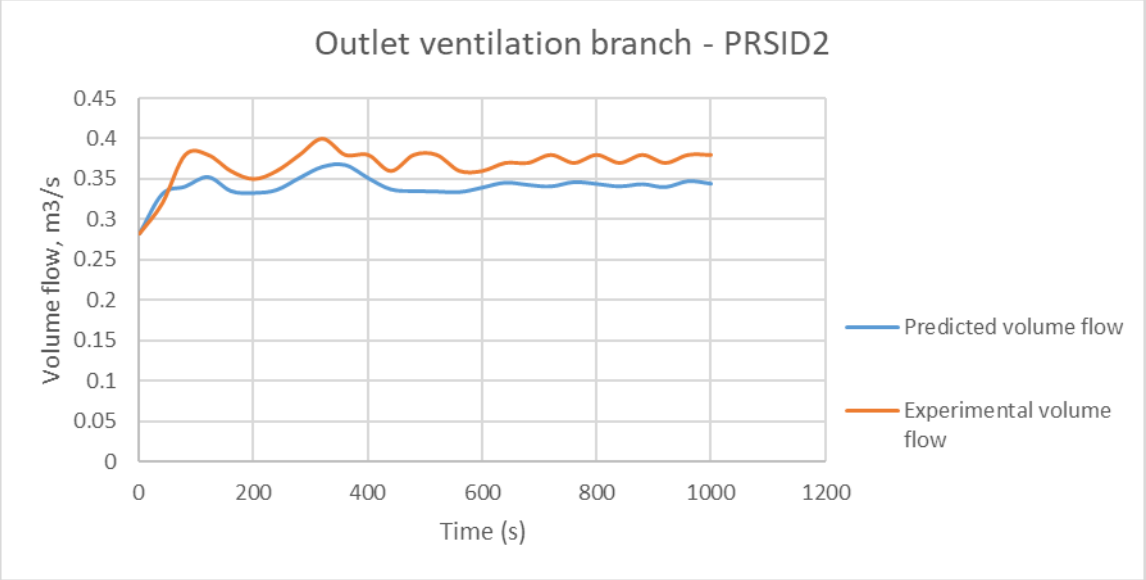

Fig. 16. Volume flow rate at outlet of ventilation branch – Predictions vs experimental data (1000 first seconds of test-PRS_SI_D2).

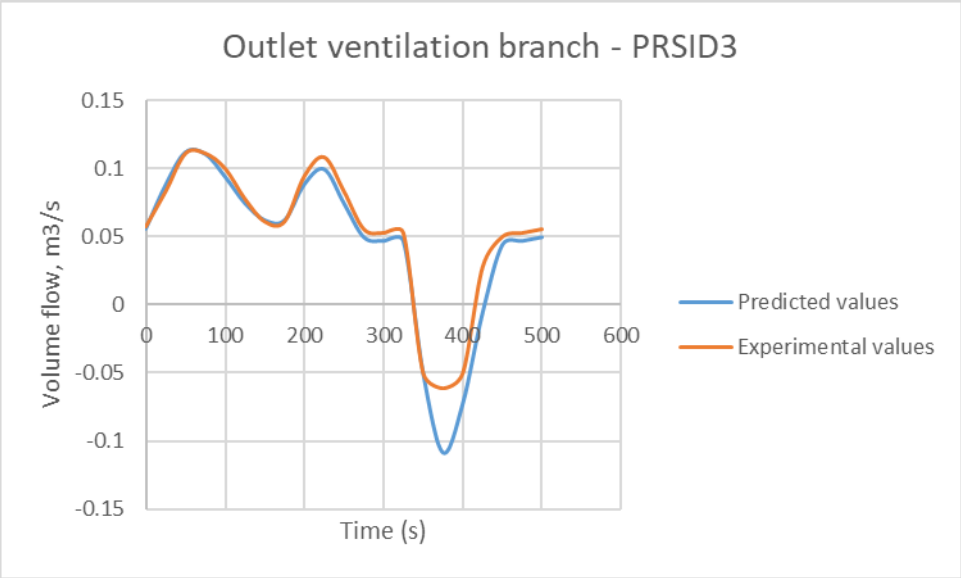

Fig. 17. Volume flow rate at outlet of ventilation branch – Predictions vs experimental data (PRS_SI_D3).

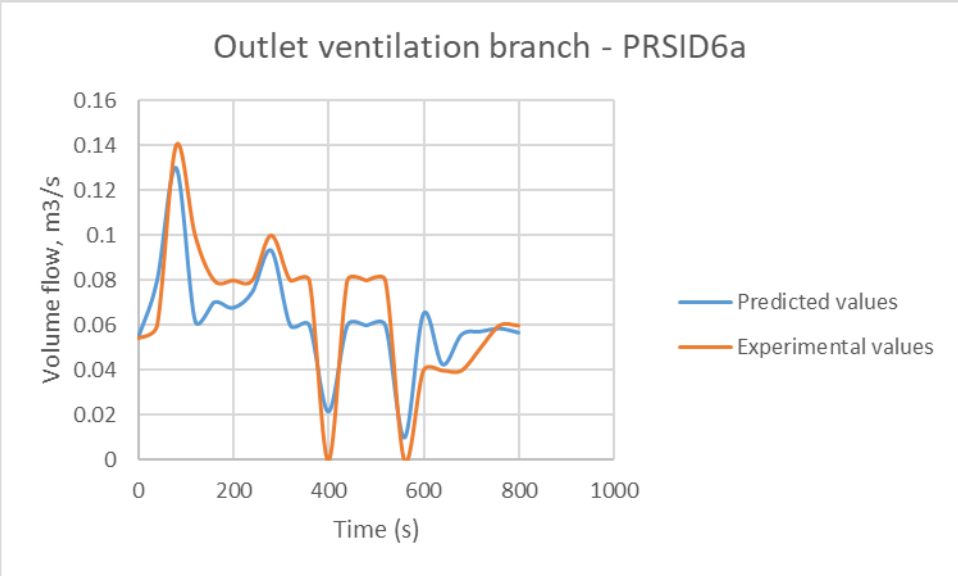

Fig. 18. Volume flow rate at outlet of ventilation branch – Predictions vs experimental data (800 first seconds of test-PRS_SI_D6a).

5.6 Gas Temperature inside Fire Compartment

Fig. 19 shows the temperature prediction at different heights in the compartment located in the north-east section of the compartment. The temperature values are predicted with a high level of accuracy with a difference of approximately 5% at steady-state. Such an accuracy is expected because of the use of a prescribed fuel mass loss rate. The temperature being underestimated explains the overestimation of the overpressure peak from Fig. 7. Temperature rise leads to an increase in pressure, therefore with the predicted temperature results lower than the experimental data, the inlet would experience a higher flow rate based on Eq. (20).

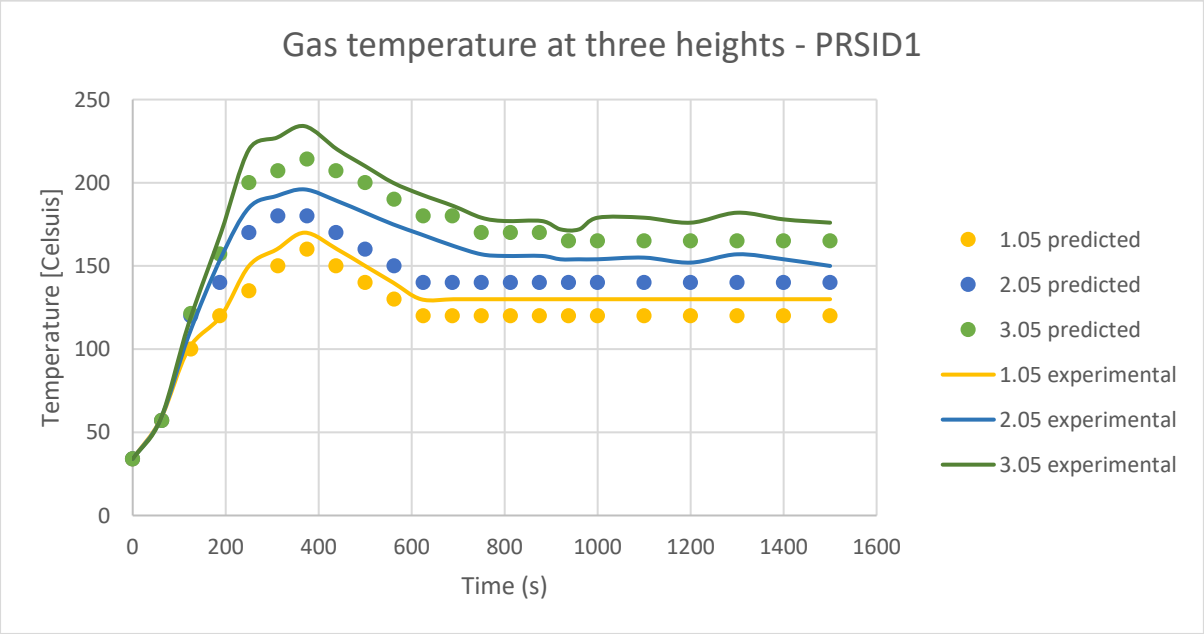

Fig. 19. Temperature values at different height in the compartment - Prediction vs Experimental data.

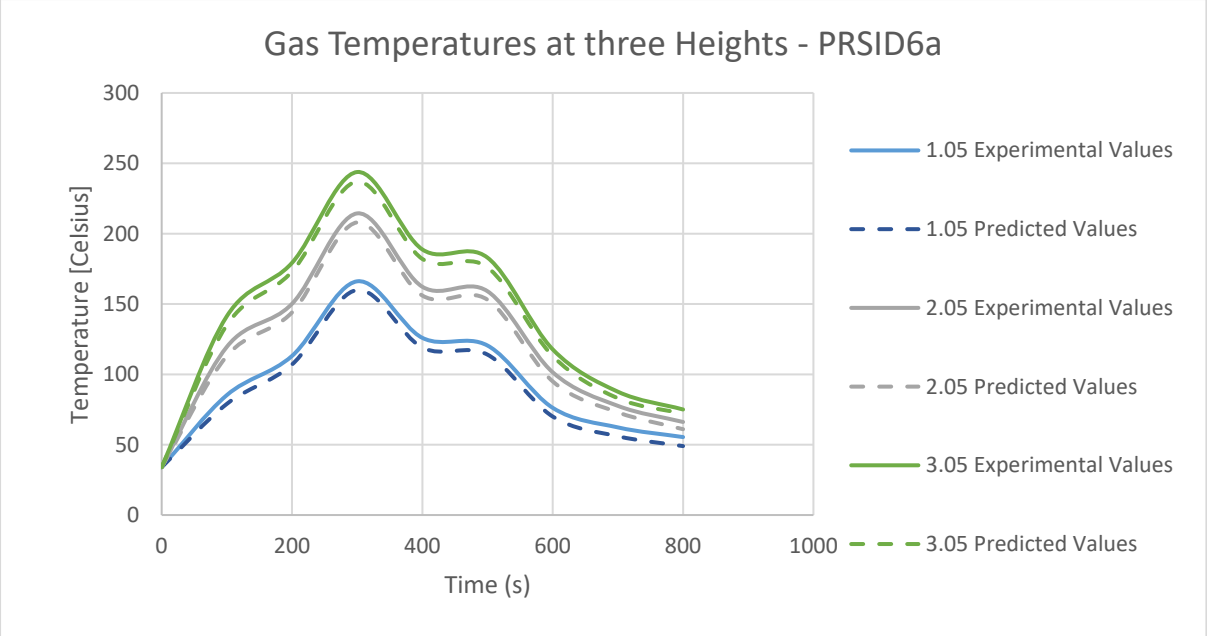

Fig. 20. Temperature values at different height in the compartment - Prediction vs Experimental data (PRS_SI_D6a).

The experimental uncertainties are set to be 2% for oxygen concentrations, 10% for flow rate, 10% for gas temperature and 10% for total heat flux. The wall temperature is set at 20% without detailed information by doubling the temperature uncertainty. The pressure measurement is also set at 30% (Audouin et al, 2011).

5.7 Oxygen concentration

Figs. 21 and 22 present the oxygen concentration at the heights of 0.8m and 3.3m in the South East quadrant of the compartment. The experimental and numerical results are in good agreement. The unsteady and steady phase of the combustion are also in good agreement. The current study makes use of prescribed fuel mass loss rate, therefore knowledge of the oxygen concentration is not significant to this study but it is important to highlight that the use of CHT does not affect the numerical oxygen concentration.

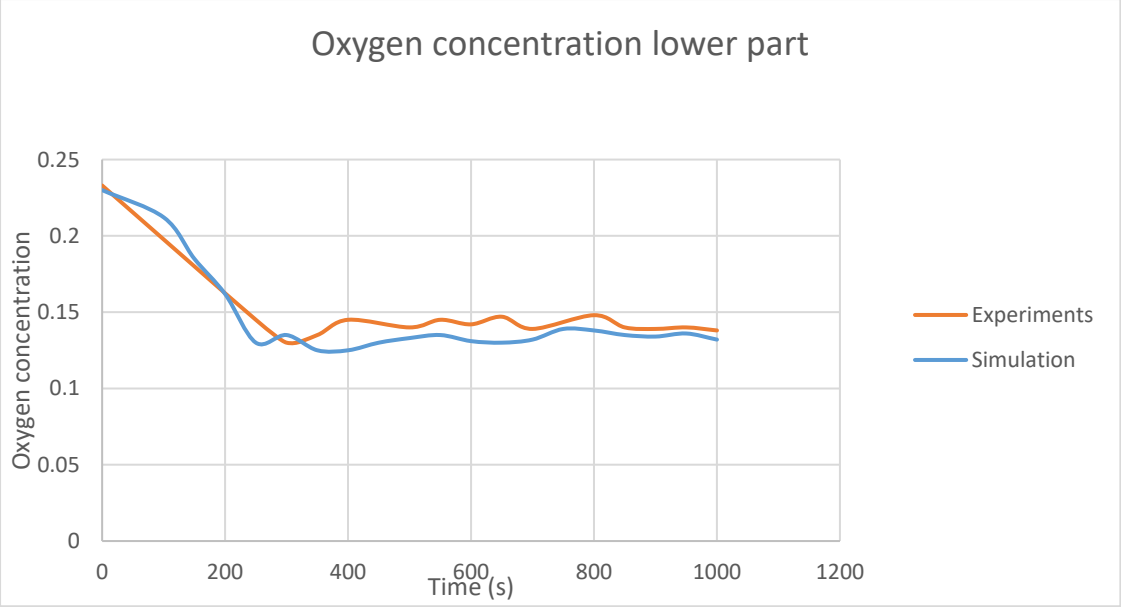

Fig. 21. Oxygen concentration at the lower part of the nuclear compartment (0.8m height).

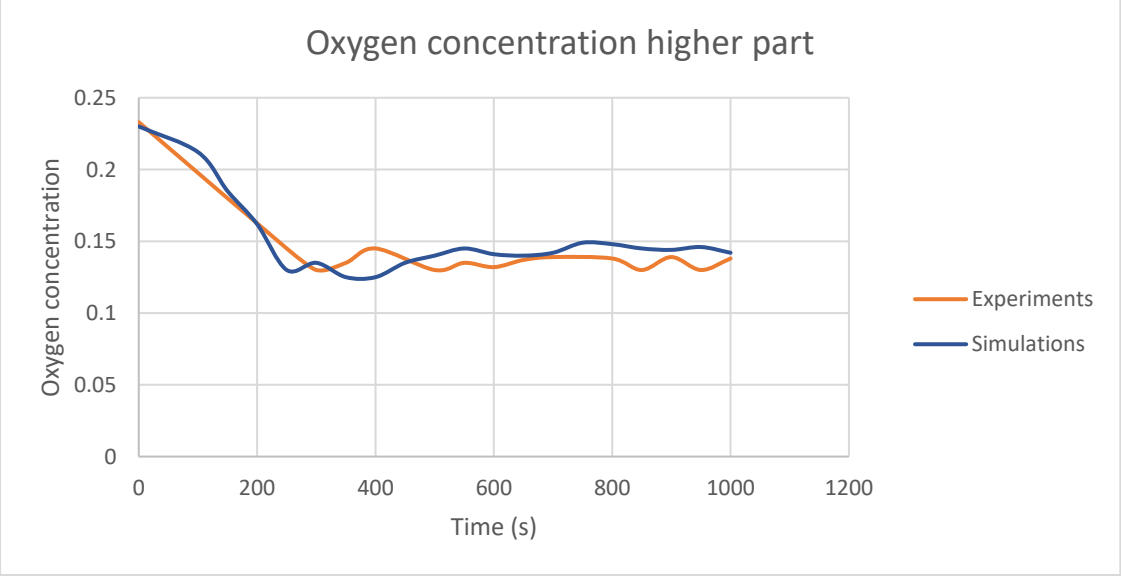

Fig. 22. Oxygen concentration at the higher part of the nuclear compartment (3.3m height)

5.8 CHT Model Validation

The validation of the CHT model is performed using the wall temperatures and heat flux values at different heights located at the north wall of the compartment (1.55m, 2.6m and 3.55m). Comparisons are made between the model's predictions and the experimental data.

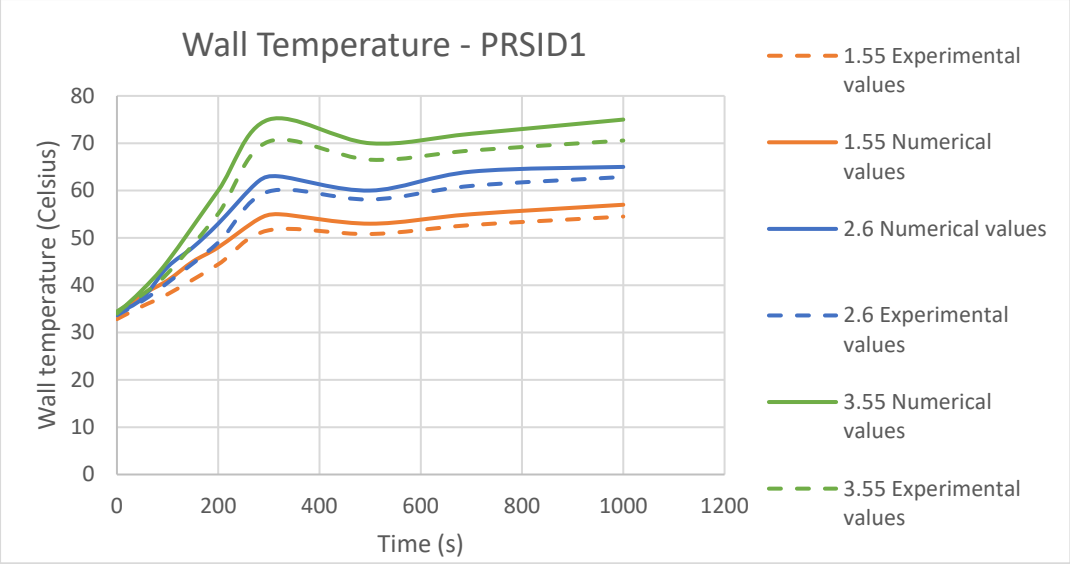

Fig. 23. Wall surface temperature for PRSID1

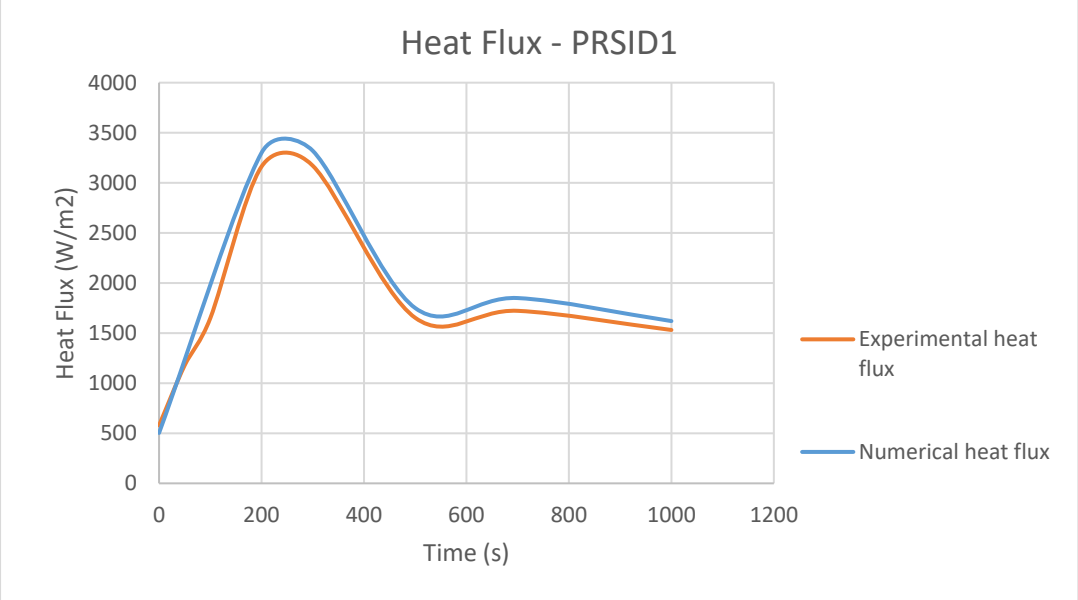

Fig. 24. Heat fluxes for PRSID1

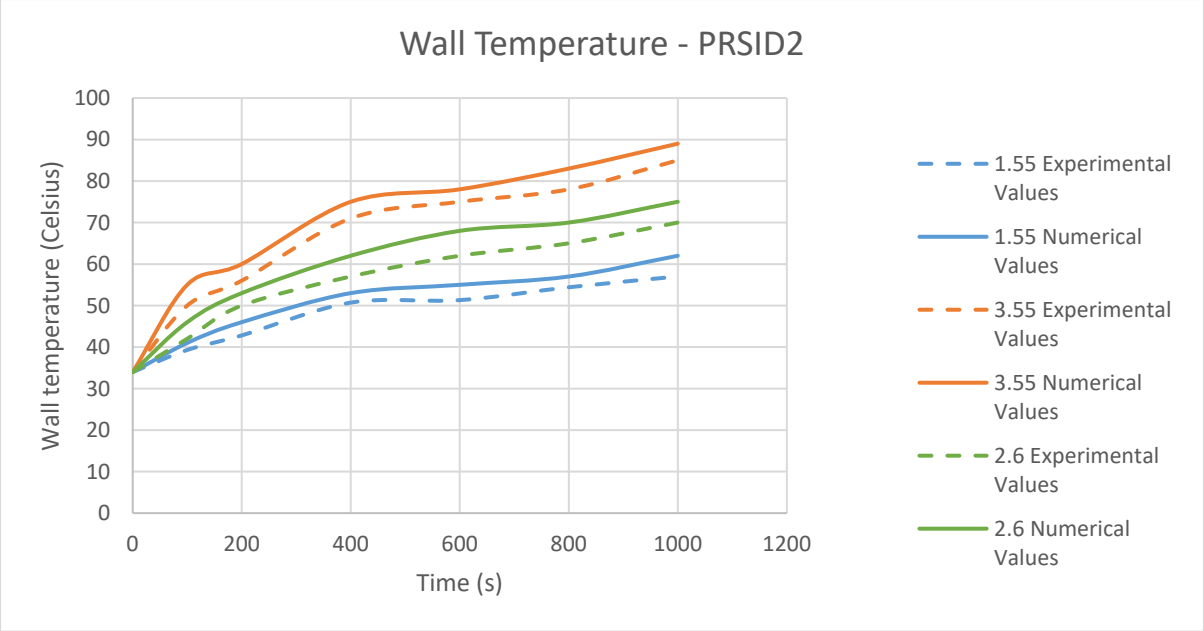

Fig. 25. Wall surface temperature for PRSID2

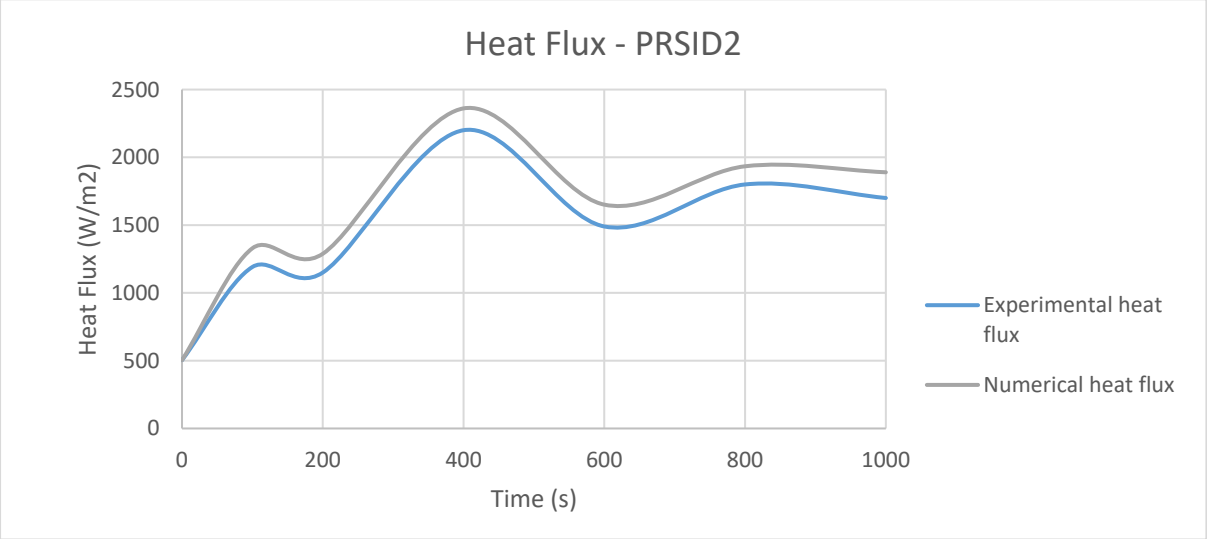

Fig. 26. Heat fluxes for PRSID2

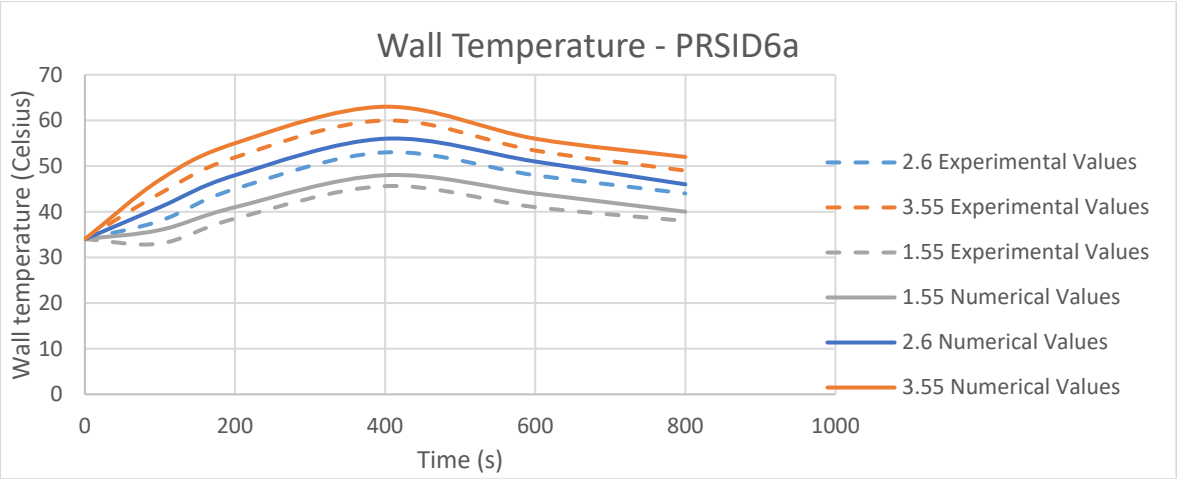

Fig. 27. Wall surface temperature for PRSID6a

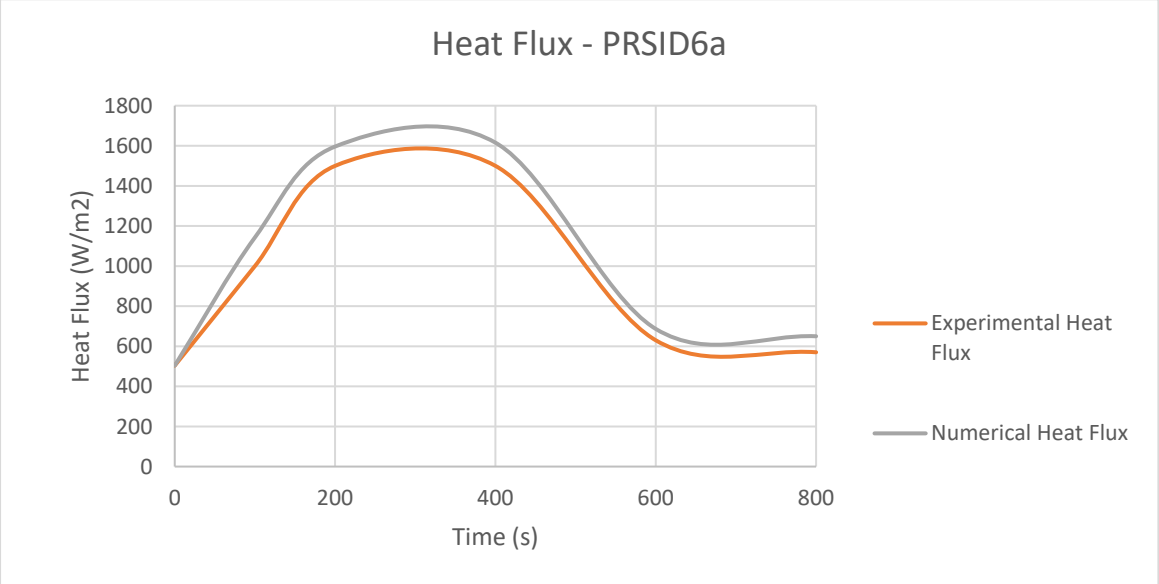

Fig. 28. Heat fluxes for PRSID6a

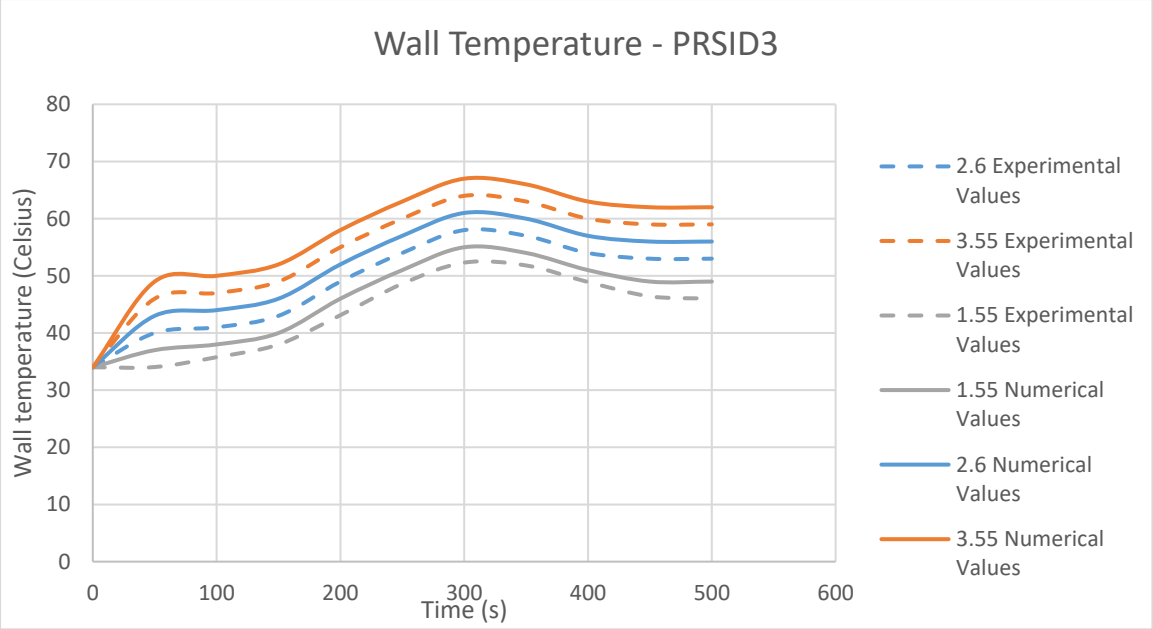

Fig. 29. Wall surface temperature for PRSID3

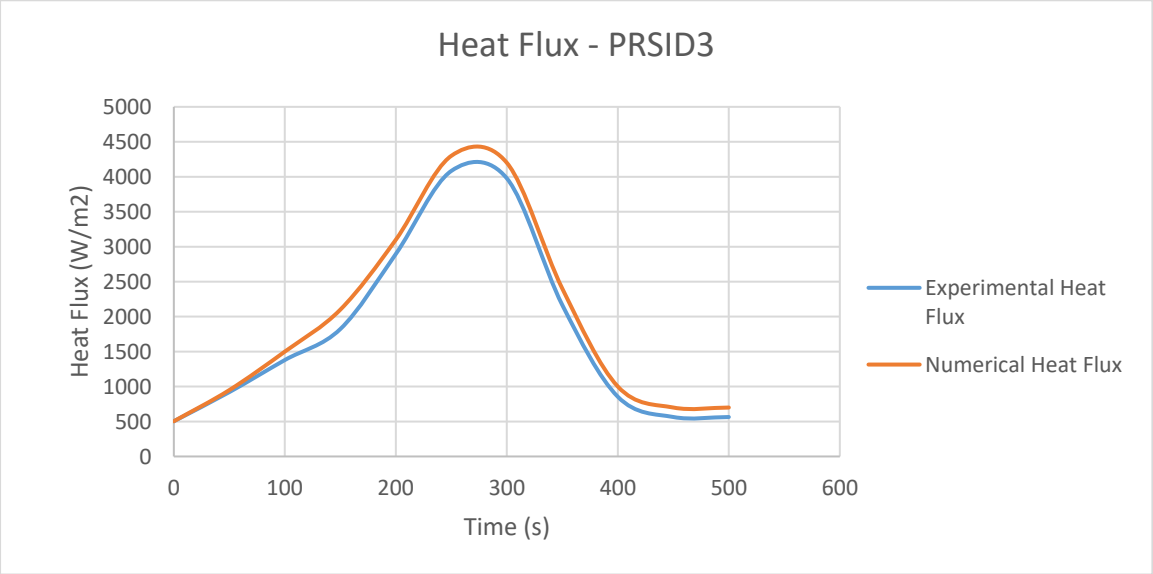

Fig. 30. Heat fluxes for PRSID3

From Figs. 23-30, the numerical and experimental simulations are in relatively good agreement. The heat flux shown is the radiative heat flux on the interface between the fluid and solid region. Using the mixed boundary condition, Eqs. 9 and 10 containing the radiative heat flux is implemented in each region to solve the temperature. The CHT model makes use of constant wall properties that could change during fire e.g. emissivity. The use of a

temperature-dependent wall property could further improve the results. From the current results, it seems clear that there are no significant advantages to using the CHT model when compared to previous studies that made use of 1D Fourier conduction equation (Lapuerta et al., 2012; Suard et al., 2011). However, the CHT model could prove essential for more complex scenarios where heat transfer between the solid and fluid plays a significant part e.g., heat transfer between ventilation ducts across two rooms.

6. Conclusion

This study aims to simulate fire behaviour in a mechanically ventilated nuclear compartment with particular attention to the pressure variation and the flow rate at the ventilation branches. An in-house version of FireFOAM, modified in the present study to implement conjugate heat transfer (CHT) and a ventilation model, is successfully used to simulate fire in a compartment with a mechanical ventilation network. The code has shown its capability to predict with relatively good agreements the pressure variations in the compartment and the flow rates at the inlet and outlet of the ventilation network. Table 6 shows the values of the pressure peaks between the experimental and simulation results. The percentage difference between the results ranges between 10-13% except for under-pressure peak for PRSID6a which was over 100%. Overall, the differences show an acceptable level of accuracy and the ability of the modified FireFOAM with the ventilation model to predict the behaviour of pressure and flow rate.

Table 6. Experimental and Simulated Over-pressure and Under-pressure peak of each four fire tests.

Test	**Experimental Over-pressure peak**	**Simulated Over-pressure peak**	**Experimental Under-pressure peak**	**Simulated Under-pressure peak**
PRSID1	420	350	-600	-400
PRSID2	300	260	-250	-200
PRSID3	2800	2500	-2500	-2400
PRSID6a	3000	2600	-3000	-800

The connection between the pressure in the nuclear compartment and the ventilation flow rates was established and it was shown how the pressure variations affect the direction of flow in the ventilation networks. The ventilation model is seen to rely on the loss

coefficients at the inlet and outlet which was calculated using the experimental data that had some discrepancies. This is because the loss coefficients are calculated from pressure measurements that carry some experimental uncertainties. This led to slight under predictions of the pressure peaks. Resolving the issue of loss coefficients by changing the values would improve the existing results. The ventilation configuration was shown to be an important parameter from PRS_SI_D6a. The position of the ventilation branch affects the burning rate of the fuel. There were other possible sources of errors identified apart from the measurement uncertainty which include the combustion and turbulence modelling. As further work to improve the code, the prediction of the fuel mass loss rate is under consideration as well as the simulations of more experimental scenarios.

The CHT model is also validated and can be seen to predict the wall temperature and heat flux values with reasonably good agreements. The scenarios in the current study do not highlight any significant difference between the use of CHT model and the previous method of 1D Fourier conduction equation. A more complex scenario could be used to highlight the significant improvement of making use of CHT model.

Acknowledgements

The authors would like to thank the UK Doctoral Training Alliance (DTA) Energy for its financial support during this project.

References

Acherar, L., Wang, H-Y., Garo, J-P., Coudour, P., 2020. Impact of air intake position on fire dynamics in mechanically ventilated compartment. Fire Safety Journal 118. https://doi.org/10.1016/j.firesaf.2020.103210.

Audouin, L., et al., 2011. Quantifying differences between computational results and measurements in the case of a large-scale well-confined fire scenario. Nuclear Engineering and Design 241(1), 18–31. https://doi.org/10.1016/j.nucengdes.2010.10.027.

Audouin, L., Pretrel, H., Rigollet, L., Le Saux, W., Rowekamp, M., 2013. OECD PRISME project: Fires in confined and ventilated nuclear-type multi-compartments – Overview and main experimental results. Fire Safety Journal 62(1), 80-101. https://doi.org/10.1016/j.firesaf.2013.07.008.

Audouin, L., Pretrel, H., Le Saux, W., 2011. Overview of the OECD PRISME project – main

experimental results. 21st International Conference on Structural Mechanics in Reactor Technology (SMIRT 21).

Bonte, F., Noterman, N., Merci, B., 2013. Computer simulations to study interaction between burning rates and pressure variations in confined enclosure fires. Fire Safety Journal 62, 125-143. https://doi.org/10.1016/j.firesaf.2013.01.030.

Cassol, F., Brittes, R., Franca, F.H.R., Ezekoye, O.A., 2014. Application of the weighted-sum-of-gray-gases model for media composed of arbitrary compositions of H2O, CO2 and soot. International Journal of Heat and Mass Transfer 79, 796-806. https://doi.org/10.1016/j.ijheatmasstransfer.2014.08.032.

Chen, Z., Wen, J., Xu, B., Dembele, S., 2014. Extension of the eddy dissipation concept and smoke point soot model to the LES framework for fire simulations. Fire Safety Journal 64, 12-26. https://doi.org/10.1016/j.firesaf.2014.01.001.

Colella, F., 2010. Multiscale Modelling of Tunnel Ventilation Flows and Fires. PhD. Politecnico di Torino.

FM Global. FireFoam, Available at: https://github.com/fireFoam-dev.

IRSN, 2013. Free Access to PRISME test results [online]. Available at: https://www.irsn.fr/EN/Research/Research-organisation/Research-programmes /prisme/ Pages/PRISME-test-results.aspx [Accessed October 10 2019].

Jiang, F., Ye, S.S., Yang, J., 2002. Design of the exhaust system in the confinement of the HTR-10. Nuclear Engineering and Design 218(1), 209-214. 10.1016/S0029-5493(02)00192-9. https://doi.org/10.1016/S0029-5493(02)00192-9.

Johansson, R., Leckner, B., Andersson, K., Johnsson, F., 2011. Account for variations in the H2O to CO2 molar ratio when modelling gaseous radiative heat transfer with the weighted-sum-of-grey-gases model. Combustion and Flame 158(5), 893-901. https://doi.org/10.1016/j.combustflame.2011.02.001.

Lapuerta, C., Suard, S., Babik, F., Rigollet, F., 2012. Validation process of ISIS CFD software for fire simulation, Nuclear Engineering Design 253, 367–373. https://doi.org/10.1016/j.nucengdes.2011.09.068.

Le, D., Labahn, J., Beji, T., Devaud, C.B., Weckman, E.J., Bounagui, A., 2017. Assessment of the capabilities of FireFOAM to model large-scale fire in a well-confined and mechanically ventilated multi-compartment structure. Journal of Fire Sciences 36(1), 3-29. https://doi.org/10.1177/0734904117733427.

Le Saux, W., Prétrel, H., Such, J.M., 2005. Experimental study of the burning rate behaviour of a pool fire in confined and ventilated compartment, in Proceeding of the 9th International Seminar on Fire Safety in Nuclear Power Plants And Installations (SMIRT 18 - Post Conference).

Lin, H., Ferng, Y.M., Hsu, W.S., 2009. Investigating the effect of computational grid sizes on the predicted characteristics of thermal radiation for a fire. Applied Thermal Engineering 29 (11-12), 2243-2250. https://doi.org/10.1016/j.applthermaleng.2008.11.010.

Magnusen, B.F., Hjertager, B.H., 1977. On mathematical modelling of turbulent combustion with special emphasis on soot formation and combustion. Symposium International on Combustion 16(1), 719-729. https://doi.org/10.1016/S0082-0784(77)80366-4.

McGrattan, K.B., Floyd, J.E., Forney, G.P., Howard, H.R., Hostikka, S., 2003. Improved Radiation and Combustion Routines for a Large Eddy Simulation Fire Model. Fire Safety Science 7, 827-838. doi:10.3801/IAFSS.FSS.7-827.

McGrattan, K., Hostikka, S., McDermott, R., Floyd, J., Weinschenk, C., Overholt, K., 2015. Fire Dynamics Simulator Technical Reference Guide Volume 1: Mathematical Model, NIST special publication 1018-1, Sixth Edition. National Institute of Standards and Technology (NIST), Gaithersburg, MD.31

Menom, S., Yeung, P., Kim, W., 1996. Effect of subgrid models on the computed interscale energy transfer in isotropic turbulence. Computational Fluids 25(2), 165-180. https://doi.org/10.1016/0045-7930(95)00036-4.

Nasr, A., Suard, S., El-Rabii, H., Gay, L., Garo, P, J., 2011. Fuel mass-loss rate determination in a confined and mechanically ventilated compartment fire using a global approach. Combustion Science and Technology 183(12),1342–1359. https://doi.org/10.1080/00102202.2011.596174.

Nuclear Energy Agency, 2016. Event Combinations of Fire and Other Events.

Perez Segovia, J.F., Beji, T., Merci, B., 2017. CFD Simulations of Pool Fires in a Confined and Ventilated Enclosure Using the Peatross–Beyler Correlation to Calculate the Mass Loss Rate, Fire Technology 53(4), 1669-1703. https://doi.org/10.1007/s10694-017-0654-2.

Prétrel, H., Querre, P., Forestier, M., 2005. Experimental study of burning rate behaviour in

confined and ventilated fire compartments. Fire Safety Science 8, 1217-1228. doi:10.3801/IAFSS.FSS.8-1217.

Prétrel, H., W. Le Saux, and L. Audouin, 2012. Pressure variations induced by a pool fire in a well-and force-ventilated compartment. Fire Saf. J. 52, 11–24. https://doi.org/10.1016/j.firesaf.2012.04.005.

Sikanen, T., Hostikka, S., 2017. Predicting the heat release rates of liquid pool fires in mechanically ventilated compartments Fire Safety Journal 91, 266-275. https://doi.org/10.1016/j.firesaf.2017.03.060.

Sikic, I., 2018. Radiative Heat Transfer for Modelling Fire and Fire Suppression. PhD Thesis, University of Warwick, UK.

Sikic, I., Dembele, S., Wen, J., 2019. Non-grey radiative heat transfer modelling in LES-CFD simulated methanol pool fires. Journal of Quantitative Spectroscopy & Radiative Transfer 234, 78–89. https://doi.org/10.1016/j.jqsrt.2019.06.004.

Smith, T.F., Shen, Z.F., Friedman, J.N., 1982. Evaluation of coefficients for the weighted sum of gray gases model. ASME Journal Heat Transfer 104(4), 602-608. https://doi.org/10.1115/1.3245174.

Suard, S., Forestier, M., Vaux, S., 2013. Toward predictive simulations of pool fires in mechanically ventilated compartments. Fire Safety Journal 61, 54–64. https://doi.org/10.1016/j.firesaf.2013.08.010.

Suard, S., Lapuerta, C., Babik, F., Rigollet, F., 2011 Verification and validation of a CFD model for simulations of large-scale compartment fires. Nuclear Engineering Design 241 (9), 3645–3657. https://doi.org/10.1016/j.nucengdes.2011.08.012.

Versteg, H.K., Malalasekera, W., 2007. An Introduction to Computational Fluid Dynamics: The Finite Volume Method. Pearson Education Limited, 2nd edition.

Wahlqvist, J., Van Hees, P., 2013. Validation of FDS for large-scale well-confined mechanically ventilated fire scenarios with emphasis on predicting ventilation system behaviour. Fire Safety Journal 62(1),102-114. https://doi.org/10.1016/j.firesaf.2013.07.007.

Wahlqvist, J., Van Hees, P., 2016, Implementation and validation of an environmental feedback pool fire model based on oxygen depletion and radiative feedback in FDS. Fire Safety Journal 85, 35–49. https://doi.org/10.1016/j.firesaf.2016.08.003.

Zigrang, D., Sylvester, N., 1982. Explicit approximations to the solution of Colebrook's

friction factor equation. AlChe Journal 28(3), 514-515. https://doi.org/10.1002/aic.690280323.